SJSU Annual Program Assessment Form
Academic Year 2015-2016

Department: Meteorology and Climate Science
Program: MS in Meteorology
College: Science
Program Website: www.sjsu.edu/meteorology
Link to Program Learning Outcomes (PLOs) on program website:PLO BS Climate
Program Accreditation (if any):
Contact Person and Email: Alison Bridger email:alison.bridger@sjsu.edu
Date of Report: June 1, 2016

Part A

1. **List of Program Learning Outcomes (PLOs)**

   The PLOs for the Meteorology and Climate Science program follow the standards accepted by the American Meteorological Society (AMS: BS in Meteorology recommendations). The roadmap for the MS in Meteorology is consistent with most universities that grant graduate degrees. Beginning graduate students are strongly encouraged to take METR 202 (Research Methods in Meteorology). The students take three required courses: METR 205 (Advanced Atmospheric Dynamics), METR 215 (Advanced Physical Meteorology), and METR 240 (Numerical Modeling). The department periodically offers a wide range of elective courses, which include topics such as turbulence, fire weather, parameterization in numerical models, and advanced synoptic meteorology. The program requires each student to complete a thesis based on research.

   The PLOs for the BS Meteorology – Concentration in Climate Science are:

   1. Be able to conduct an independent research project, and communicate the results in written and oral form in acceptable professional formats.
   2. Be able to explain meteorological phenomena in terms of advanced physical and dynamic concepts.
   3. Understand and be able to apply advanced numerical methods to solve atmospheric and climate science problems

2. **Map of PLOs to University Learning Goals (ULGs)**

		MS METEOROLOGY			
university		program	PLO-1	PLO-2	PLO-3
			independent research project	explain met phenomena	numerical methods
ULG-1	1.1		X	X	X
ULG-2	2.1		X	X	X
	2.2			X	
	2.3			X	
ULG-3	3.1		X	X	X
	3.2		X	X	X
ULG-4	4.1		X	X	X
	4.2		X	X	X
	4.3		X	X	X
ULG-5	5.1			X	
	5.2				
courses			thesis!!	205,215	240

3. Alignment – Matrix of PLOs to Courses

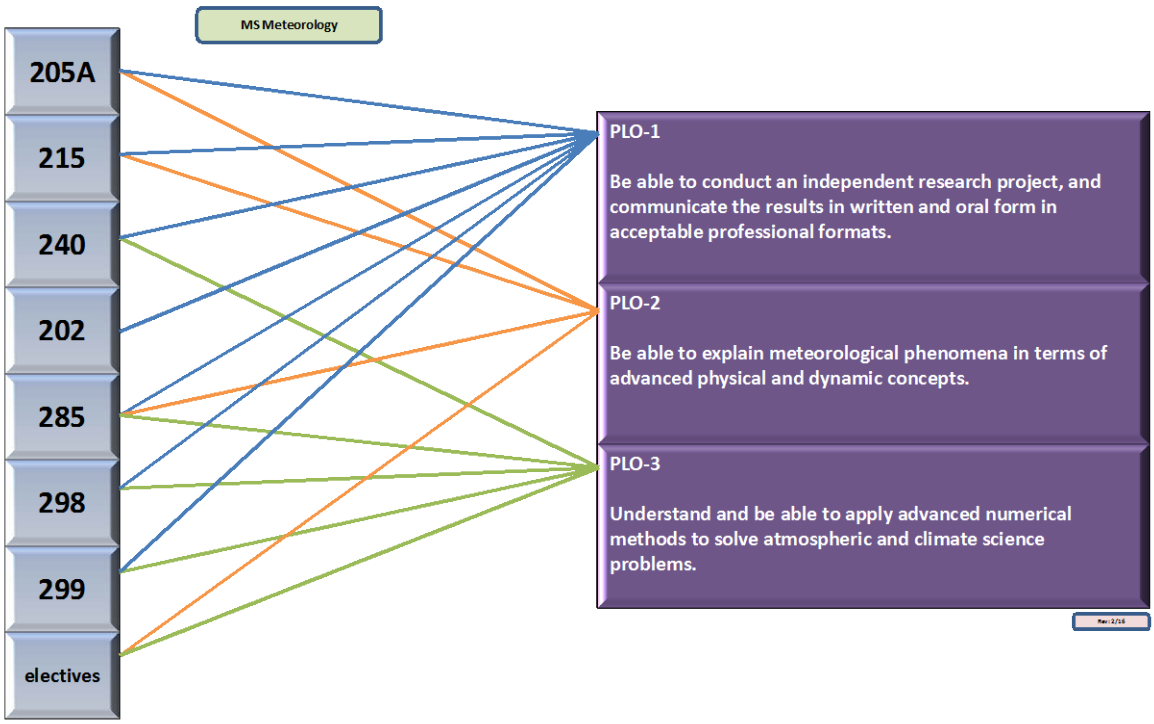

4. Planning

	AY 13-14	AY 14-15	AY 15-16	AY 16-17	AY 17-18
PLO 1					
PLO 2					
PLO 3					

5. Student Experience

a. Most classes in the program maintain a CANVAS Course Management System website where the syllabus is readily available and instructors use the tools to communicate with the students.
b. The students do not have an opportunity to provide feedback on the PLOs or on the assessment activities.

Part B

6. Assessment Data and Results

We assess PLO 2 in this assessment cycle: Be able to explain meteorological phenomena in terms of advanced physical and dynamic concepts. We assess PLO 2 using two courses: METR 205 (Atmospheric Dynamics Fall 2015), and METR 240 (Numerical Modeling, Spring 2016)

METR 205

Catalog Description METR 205 (Advanced Atmospheric Dynamics):
Dynamics of synoptic- and large-scale flows. Quasi-geostrophic theory and applications to mid-latitude storms; atmospheric waves; barotropic and baroclinic instabilities; energetics of atmospheric systems; wave-mean flow interactions; dynamics of the general circulation; tropical and stratospheric dynamics.

Learning objectives are developed to assist students in understanding the main goals of the course. During the semester, teaching and learning activities are designed with these objectives in mind. Assessment activities play the role of measuring to what level students achieved these learning objectives. The particular learning objectives for this course include:

- To understand the fundamentals and limits of quasi-geostrophic theory in describing atmospheric circulations.
- To develop experience using wave perturbation techniques in solving dynamical systems.
- To develop skills and experience using the concepts of wave-mean flow interaction.
- To develop an appreciation for the averaging techniques used to study the general circulation.
- To develop experience analysing atmospheric data (i.e., observations and model output) using modern visualization and analysis techniques.
- To develop experience researching and presenting topics in atmospheric dynamics.

METR 240

Catalog Description METR 240 (Numerical Modeling):
Numerical analysis and prediction in meteorology. Numerical methods and their errors; finite-difference and spectral methods; atmospheric models.

NWP is the process of using numerical techniques to solve the differential equations that represent the dynamics of the atmosphere including the physical processes such as thermodynamics, radiative transfer, and turbulence.

Learning Objectives:
Upon completion of this course, students should be able to:

- Understand how an NWP model is configured and run to solve the differential equations governing the atmosphere to produce a forecast.
- Utilize basic forecast verification techniques to evaluate NWP model forecasts.
- Understand the predictability of the atmosphere and methods developed to address predictability such as ensemble forecasting and data assimilation.
- Run the WRF model and analyze its output.

The expected learning outcomes will be assessed through following:

- Two graded homework assignments;
- Project results reported in a paper along with an oral presentation.

Both courses, METR 205 and METR 240 require students to understand the fundamental concepts of atmospheric circulation and demonstrate that understanding through exams, homework assignments, and projects that require papers and presentations. The assignments and projects require computer programming.

METR 205 (Advanced Dynamics) emphasizes the fundamental concepts and running models that are simple in comparison to those that are used in METR 240 (Numerical Modeling). The computer

environment required to run the simpler models in METR 205 is also much simpler than that is required to run the Weather Research and Forecasting (WRF) model used in METR 240.

In METR 205, 10 students participated; the final grade distribution was 4A's, 5B's and 1C. In METR 240, 8 students participated and all were among the 10 who had been in MER 205. The final grade distribution was 4 A's and 4 B's. The same 4 students earned A's in both classes and the 4 who earned B's in METR 205 earned B's in METR 240.

7. Analysis

Most careers in Meteorology and Climate Science require strong programming skills while at the same time require understanding difficult concepts. One clear difference between the two groups (A's and B's in both classes) was their programming skills. The better programmers generally understood the difficult concepts better and were able to completed more advanced projects. Examples of and A and a B project from both classes are attached as appendices.

8. Proposed changes and goals

Students who take either of these two courses should be required to demonstrate programming skill, by showing a history of success in other classes requiring programming, passing a test, or taking an intense short course in programming in a modern programming language (e.g. Python).

Part C

Overall, we are very happy with our graduate program. We have high standards (as recognized by colleagues at other institutions), and high expectations, and we generally have very positive outcomes.

Proposed Changes and Goals	**Status Update**
Assess programming skills	
Complete programming training for those who don't pass assessment.	

Appendices

1. Paper from METR 205 graded ‘A’
2. Paper from METR 205 graded ‘B’
3. Paper from METR 240 graded ‘A’
4. Paper from METR 240 graded ‘B’

1. **Impacts of Geoengineering on the Quasi-Biennial Oscillation**

Student who received ‘A’ in METR 205
San Jose State University, San Jose, California

1. Abstract

The quasi-biennial oscillation (QBO) is an atmospheric feature in the tropical stratosphere which is marked by downward propagating variations in both zonal wind speeds and direction. A prominent solar radiation management proposal has been to inject massive amounts of liquid sulphate particulates into the lower stratosphere in the tropics. A 2-D model created by Cordero and Nathan (2000) is utilized to examine how the QBO may be affected by temperature and ozone perturbations induced by the addition of sulphate particulates. These perturbations are taken from Tilmes et al. (2009) who determined via model output many implications of this geoengineering project. Four separate runs are performed: a control run (non-geoengineered), a geoengineered run (applied both geoengineered temperature and ozone perturbations), and two test runs where only one of the two aforementioned perturbations were applied. Analysis suggests an accelerated QBO oscillation due to geoengineering would be approximately 1.5 times faster than an unperturbed environment due to enhanced thermal damping from both temperature and ozone perturbations. The results reveal an acute sensitivity of the QBO to such external forcings, suggesting such geoengineering actions should be avoided if possible.

2. Introduction

Due to an ongoing standstill in the international community towards implementing major cut-backs in carbon emissions globally, projects aimed to offset the negative impacts of global warming have been suggested. One prominent

---

* Corresponding author address: John J. D'Alessandro,
San Jose State University, Dept. of Meteorology and Climate Science, San Jose, CA
630-665-6584; email: john.dalessandro@sjsu.edu

geoengineering concept considers injecting large quantities of liquid sulphate particles into the lower stratosphere over the tropics.
Sulphate aerosols have a high albedo, which would theoretically act to increase the global albedo by being transported via the Brewer-Dobson Circulation (Tuck et al. 2008). In theory, this solar radiation management technique would offset global warming trends.
Sensitivities of this geoengineering idea have been studied and multiple consequences from implementing such a campaign have been noted (Robock 2006 and Kalidini et al. 2015). It is imperative that a strong understanding of the sensitivities and forcings of such a campaign be established if it were ever to be carried out. The Quasi-Biennial Oscillation (QBO) is an atmospheric feature which resides in the stratosphere over the tropics and is noted by a quasi-periodic variation of zonal winds. Due to its interconnectedness with various earth systems, it is essential to understand the impacts stratospheric sulphate injections (SSI) could have on the QBO.

3. Methodology

This study utilizes the Cordero and Nathan (2000) 2D model which simulates the QBO and accounts for an explicit treatment of ozone, though it does not treat the chemistry of the atmosphere. It treats the atmosphere as a zonally averaged system. The model's domain is from 0^{O} latitude to approximately +/- 40^{O} latitude, and extends from 17 km to 34 km vertically. Boundary conditions at the domain's limits have u, v, w, and geopotential set equal to 0. For additional details of the model, the reader is instructed to turn to Cordero and Nathan (2000).
To account for impacts of SSI, temperature and ozone perturbation fields within the Cordero and Nathan model are altered to account for resulting impacts of SSI. The temperature and

ozone perturbations are taken from Tilmes et al. (2009), which performed a study examining climate sensitivities to SSI. They used the Whole Atmosphere Community Climate Model, a coupled chemistry model to perform their study. For their aerosol input considering sulphate particles, they pull the same initial conditions from Rasch et al. (2008), which performed multiple sensitivity test with varying initial sulphate aerosol conditions. Tilmes et al. only used the Volc2 sulphate initial conditions which inputs two teragrams of sulphate aerosols yearly and uses larger particle sizes (effective radius: 0.43 um), which is shown to be more realistic as smaller particles are expected to quickly coagulate (Tilmes et al. 2009). Figure 1 highlights ozone and temperature fields taken from the difference of their control case (normal conditions) and geoengineered case.

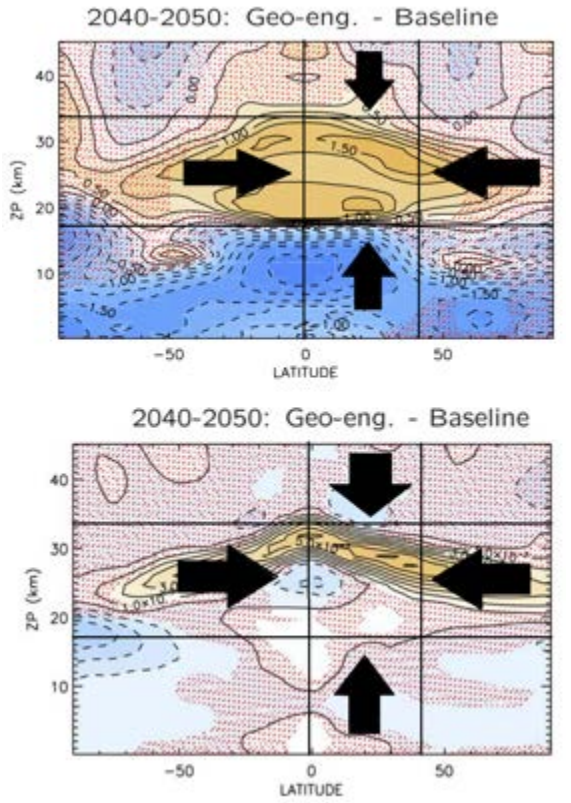

Figure 1: Top: Temperature (K) and Bottom: Ozone mixing ratio (dimensionless) differences between the Tilmes et al. geoengineering run and control run (Tilmes et al. 2009)

The gridded portions contain the same boundary fields as the Cordero and Nathan model. The anomalies shown were applied to initial temperature and ozone perturbation fields in the Cordero and Nathan model as shown in Figure 2. Four simulations were performed; Table 1 lists the different conditions for each run.

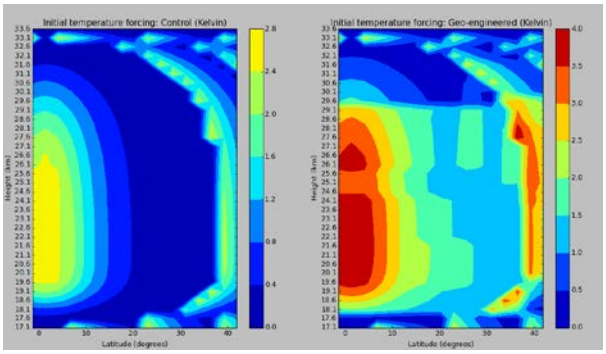

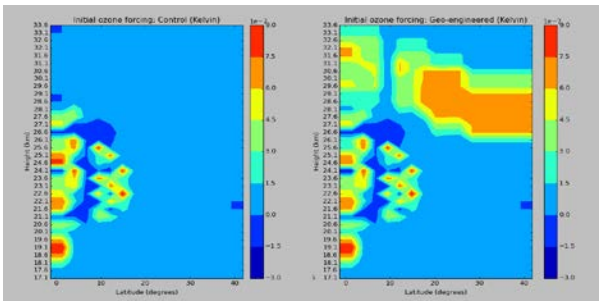

Figure 2: Top: Initial temperature perturbation field (left) and updated temperature field taken from temperature anomalies in the Figure 1 temperature field (right). Bottom: The same procedure imposed on ozone field.

Simulation	Temperature Perturbation	Ozone Perturbation	QBO Oscillation Duration (Via FFT)
Control	Initial	Initial	27 months
Geoengineered	Perturbed	Perturbed	17 months
Temp. Pert.	Perturbed	Initial	24 months
Ozone Pert.	Initial	Perturbed	22 months

Table 1: List of simulations performed: the fields perturbed, and associated QBO cycle durations derived via Fast Fourier Transforms (FFT).

3.

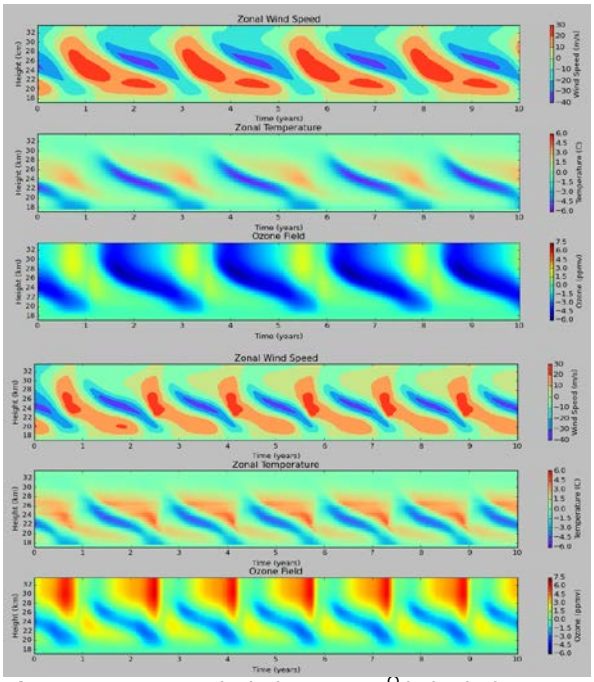

Figure 2: Top: Zonal winds at +1.35^{O} latitude for ten Years. Bottom: Similar conditions for geoengineered run.

3. Results

Initial comparisons between the control run and geoengineered run reveal a decrease in the duration of the QBO oscillation (Figure 2). A fast fourier transform (FFT) is applied to each simulation by examining the oscillating pattern of zonal winds at both 26 km and +1.35^{O} latitude (See Table 1). It can be seen that the increase in the QBO oscillation due to SSI perturbations is approximately 1.5 times faster. However, previous studies relating the QBO to sulphate aerosol perturbations suggest a *slower* QBO is expected from a warmer stratosphere (Thomas et al. 2009). Both perturbations result in net warming upon the tropical stratosphere, however, findings suggest the *stably stratified nature of the perturbation*, seen in both perturbed fields but attributed primarily to the ozone perturbation due to the faster QBO oscillation compared to the temperature perturbation, is the reason for the increased QBO oscillation.

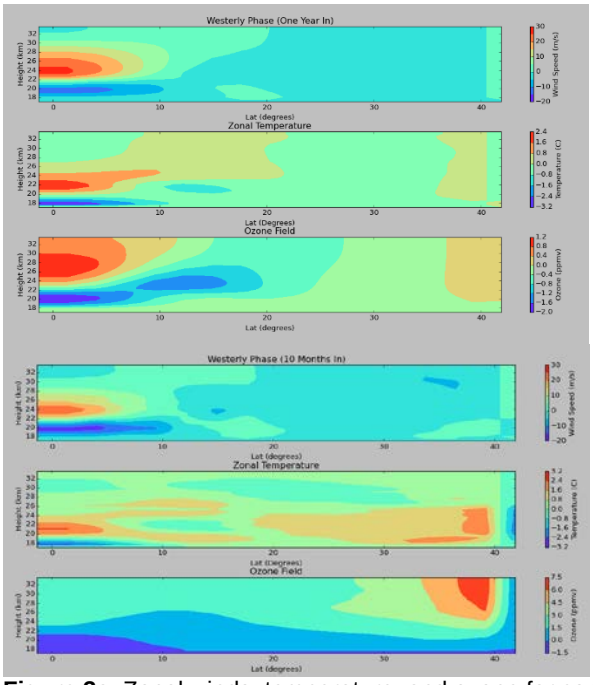

Figure 3a: Zonal winds, temperature, and ozone for control run (top) and geoengineered run (bottom) for first observed westerly phases in QBO simulations.

Westerly and Easterly phases were observed and compared for both control and geoengineered runs (Figure 3a and Figure 3b, respectfully).
Westerlies are observed to decrease for the geoengineering run, which corresponds to the reduced meridional temperature gradient as satisfied via the thermal wind relation (Shown below).

$$\frac{\partial u}{\partial z} = \frac{-R}{H\beta}\frac{\partial^2 T}{\partial y^2}$$

This observation provides validation for correctly integrating the geoengineered perturbations into the model, as reduced westerlies are expected from a weaker meridional temperature gradient. Examination of the Easterly phase reveals a very large and tight vertical thermal gradient in the geoengineered simulation. The EP flux divergence is shown for both easterly and westerly phases in Figure 4. The EP flux contribution from the Rossby-Gravity wave

4.

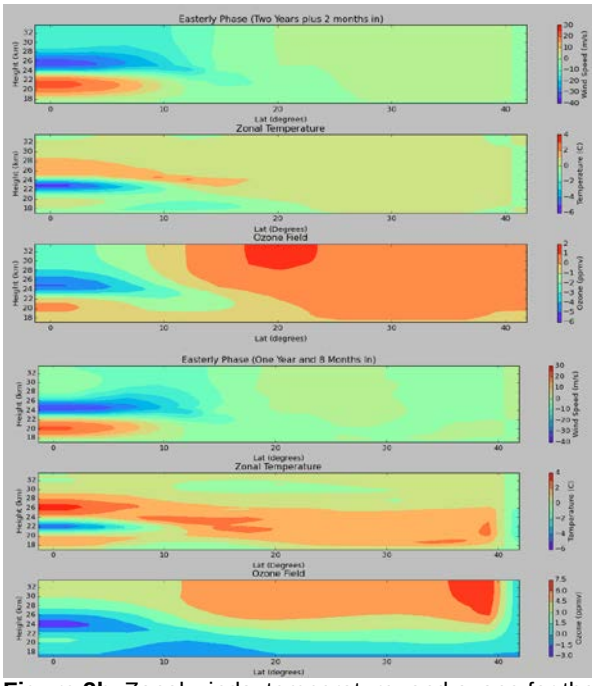

Figure 3b: Zonal winds, temperature, and ozone for the control run (top) and geoengineered run (bottom) for first observed easterly phases in QBO simulations.

activity is ~5 times larger for the geoengineered run. Secondary circulations are generally noted to offset potential variances in the zonal winds, by which those responses are dependent on the thermal wind relation (Holton 4th ed.).

Examination of time dependent vertical and meridional wind velocities at +1.35^{O} and +6.75^{O} latitude, respectfully, provide evidence for this strong residual circulation response which is only observed for the easterly phase (Figure 5).

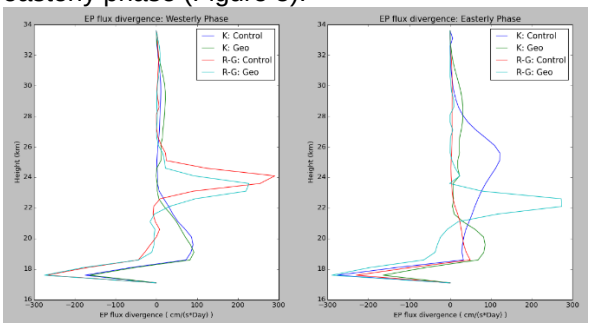

Figure 4: EP flux divergence shown for easterly and westerly phases (same cases as Figure 3a & 3b). Contributions from Kelvin (K) and Rossby-Gravity waves (R-G) are treated separately.

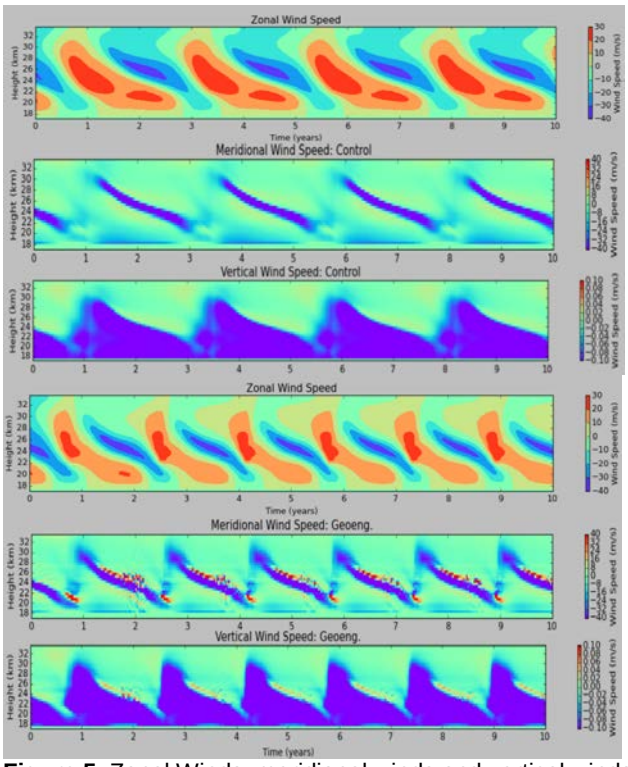

Figure 5: Zonal Winds, meridional winds and vertical winds for the control run (top) and geoengineered run (bottom). Note the strong secondary circulations induced only in the easterly phase.

Thus, it is hypothesized the strong circulation acts to induce a further reduced meridional temperature gradient to prevent zonal flow from increasing, due to Rossby-Gravity waves both being very sensitive to temperature perturbations and providing eastward momentum by their nature.

4. Conclusion

Analysis utilizing the Cordero and Nathan (2000) model to determine SSI impacts on the QBO suggests an increase in the periodicity of the QBO oscillation is expected due to increased momentum forcings. These momentum forcings arise primarily from Rossby-Gravity wave activity in the easterly phase interacting with an enhanced vertical thermal gradient which provides increased thermal damping in the region.

5.

This enhanced thermal damping is thought to result from the enhancement of a stably stratified environment due to both ozone and temperature perturbation fields as taken from Tilmes et al. (2009). Both ozone and temperature perturbations are positive anomalies, with the strongest anomalies in the middle to upper stratosphere. Observations of the secondary circulation (v and w fields) during the easterly phase provide evidence for this.

Further research is required to account for the chemical and microphysical interactions within the stratosphere, as the Cordero and Nathan model does not account for either.

The subjective nature of this study must also be acknowledged, as temperature and ozone perturbations were treated and input visually, which provides the potential for human error. However, the stability imposed by the perturbations would still be expected even with an imperfect implementation of both perturbation fields, so long as the stably stratified nature of the perturbation fields is captured.

5. Appendix

1. Cordero, E. C. and T. R. Nathan. 2000: The Influence of Wave– and Zonal Mean–Ozone Feedbacks on the Quasi-biennial Oscillation. *J. Atmos. Sci.*, 57, 3426-3442.

2. Holton, J. 2004: An Introduction to Dynamic Meteorology, 4th ed.

3. Kalidindi, S., Bala, G. A. Modak, K. Caldeira. 2015: Modeling of solar radiation management: a comparison of simulations using reduced solar constant and stratospheric sulphate aerosols. *Clim. Dyn.*, **44**, 2909-2925.

4. Rasch, P. J., P. J. Crutzen, D. B. Coleman. 2008: Exploring the geoengineering of climate using stratospheric sulfate aerosols: The role of particle size. *Geophys. Res. Lett.*, **35**, L02809.

5. Robock, A. 2008: 20 Reasons why geoengineering may be a bad idea. *Bulletin of the Atomic Scientists*, **64**, 14-18.

6. Thomas, M. A., M. A. Giorgetta, C. Timmreck, H. F. Graf, G. Stenchikov. 2009: Simulation of the climate impact of Mt. Pinatubo eruption using ECHAM5 – Part 2: Sensitivity to the phase of the QBO and ENSO. *Atmos. Chem. Phys.,* **9**, 3001-3009.

7. Tilmes, S., R. R. Garcia, D. E. Kinnison, A. Gettelman, P. J. Rasch. 2009: Impact of geoengineered aerosols on the troposphere and stratosphere. *J. Geophys. Res*., **114**, D12305.

8. Tuck, A. F., D. J. Donaldson, M. H. Hitchman, E. C. Richard, H. Tervahattu, V. Vaida, J. C. Wilson. 2008: On geoengineering with sulphate aerosols in the tropical upper troposphere and lower stratosphere. *Climate Change*, **90**, 315-331.

OZONE SUPER-RECOVERY AND THE MODELED IMPLICATIONS ON THE QUASI-BIENNIAL OSCILLATION

Student who received 'B' in METR 205

(EXTENDED ABSTRACT)

Meteorology and Climate Science Department, San Jose State University, San Jose California

Introduction

Stratospheric Ozone concentrations and their depletions became widely known to the public in the 1970's. Largely due to the felt urgency of recovering our atmospheric filter of harmful shortwave radiation, consumer choices changed, followed by policy change. This is a success story in the communication between scientists and policymakers. Still, ozone levels, by volume were reduced roughly four percent by volume from 1980 levels. Currently, stratospheric ozone is in a state of recovery. Some scientists believe that a super-recovery in stratospheric ozone is possible by up to six percent (Li 2006). While many scientists understand stratospheric ozone in its radiative absorption properties, few look at its influence on vertically propagating planetary waves. This research examines the indirect influence ozone concentrations have on tropical stratospheric winds by its capacity to modify vertically propagating planetary waves. By using a two dimensional model, the investigation aims to verify if increased ozone concentrations brought on by a super-recovery increase stratospheric zonal winds speeds and increases the oscillation period of the quasi-biennial oscillation (QBO).

The accepted theory behind the QBO is that vertically propagating planetary waves are responsible. In particular, the modification of these vertical waves allows for the zonal transfer of momentum through either dampening or amplification. Early modeling shows that Kelvin

*corresponding author address: Leo A. Bate-Campos, San Jose State University. Dept. of Meteorology & Climate Science, San Jose, CA 95192

waves and Rossby-Gravity waves can influence momentum upon stratospheric zonal winds. Nathan (1994) affirms that a diabatic heating effect from advecting ozone can modify Newtonian Cooling, a term that regulates dampening of vertically propagating winds. Later modeling by Cordero (1997) looked into the into the feedbacks of ozone on Kelvin and Rossby-Gravity waves specifically. Three elements of ozone feedbacks on the QBO are parameterized into a model including an ozone heating coefficient. The other parameterizations capture photochemical responses to diurnally induced perturbations of ozone and temperature respectively. Subsequent research by Cordero (2000) employs a modified two dimensional mechanistic model that assumes zonal averages to illustrate wave-ozone and zonal mean ozone feedbacks on the QBO. Again in this investigation, stratospheric ozone modifies Newtonian cooling which modifies the amplification or dampening of vertically propagating waves. This research employs the same model to find how ozone quantity in a super-recovery scenario may impact the QBO.

Methodology

This research alters magnitude values for stratospheric ozone. By changing both the vertical and meridional ozone gradient, a suitable change for total ozone can be established. The study does neglect, however, the largely chemical influences responsible for much of the ozone super-recovery. Austin (2006) uses a chemically coupled model to explain the recovery of stratospheric ozone as largely chemically and temperature dependent. In these model runs, the parameterizations of ozone heating and the photochemical responses to wave perturbations in ozone and temperature remain fixed, simplifying the structure of research. It has also been posited that temperature changes brought on by climate change may alter stratospheric ozone levels. This element is also left unaltered for this research.

While NOAA and 2005 IPCC maximum stratospheric ozone forecasts both display a range including values exceeding 1980 levels, neither are as bullish as Li's (2006) six percent forecast maximum. It bears mentioning that the six percent super-recovery maximum is applied homogenously

across the spatial domain of the model in this research. Real projections include an uneven distribution due to solar incident angles, for example.

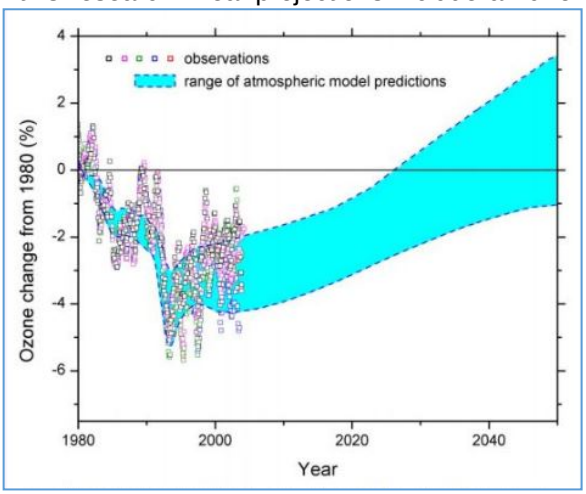

Figure 1. NOAA timeline on stratospheric ozone through 2050

Three runs of the Cordero (2000) model are conducted, modifying ozone quantity on each run. Each run is extended for a twenty year period. They intend to capture the levels of stratospheric ozone for the overall ozone low, the accepted normal at 1980 levels and the maximum forecast super-recovery levels. Due to the mechanistic nature of the employed model, runs will differ by a percentage increase from the control run instead of measured and forecast values, meaning a four percent increase for 1980 levels against the low and a ten percent increase from the maximum super-recovery to the low. This allows for a comparison, examining the result of changing ozone values on stratospheric ozone winds.

Analysis of the data measures zonal winds, temperature, and ozone levels in the stratosphere. Temperature and ozone data is collected to qualitatively assess consistencies with the zonal winds. Observations are made between the 18 kilometer and 32 kilometer vertical levels to isolate the winds relevant to the QBO.

Results

An assessment of stratospheric zonal winds is focused on. Observations of winds at the equator over time are compared. Qualitatively, all runs exhibit a similar structure with winds of a similar order of magnitude. It is also observed that the QBO period remains qualitatively indistinguishable.

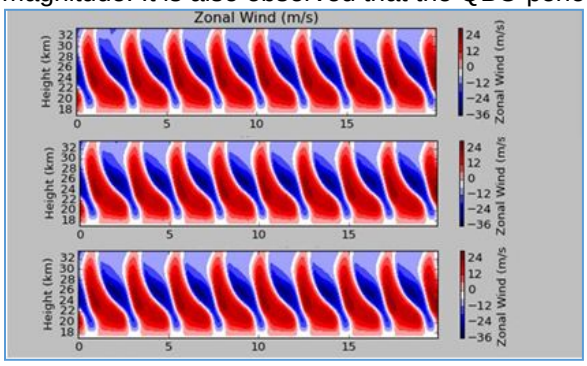

Figure 2. Zonal winds over time. Runs are displayed with the control above followed by a 4%, then 10% increase.

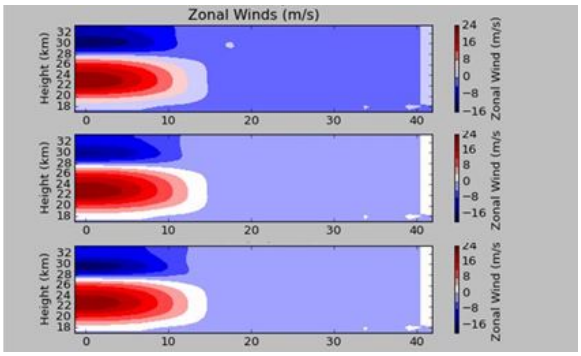

Figure 3. Zonal winds over latitudes 12 years into the run.

A difference plot offers a better qualitative comparison. Because the focus of the research compares super-recovery impacts, plots are always compared to the ten percent increase run.

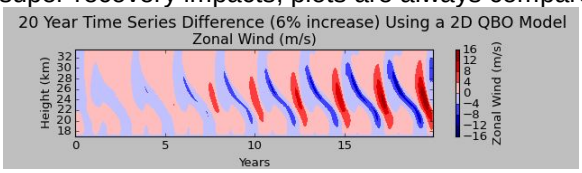

Figure 4. Zonal wind comparison between 1980 values and super-recovery values.

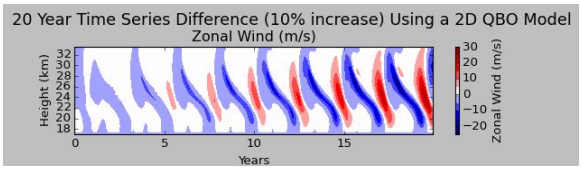

Figure 5. Zonal wind comparison between ozone low values and super-recovery levels.

Confirmation of similar structure and magnitude winds is subsequently followed by a numerical analysis. This is done by selecting the 26 km elevation for comparison. It is chosen to represent a midpoint in the QBO and capture the general pattern. A plot of wind magnitudes over time is then analyzed to find the period length in years. An analysis between the last recorded period of each run is compared to the first recorded period of its respective run. Comparison reveals that the first and last period of each run is virtually the same. For this reason, the last period length of each run is compared to different runs revealing how stratospheric ozone levels alter the period. An examination of the numbers reveals that there is virtually no change in period when the ozone low run is compared to the super-recovery. A change is observed, however between the run containing 1980 ozone levels compared to the super-recovery levels. In this comparison, the QBO period is extended almost 15 days. This is counterintuitive, assuming that the ozone magnitude change is less when more period change is observed. This likely has to do with the non-linear nature of the system and tells us that the negative feedbacks tend to cancel out positive feedbacks when ozone magnitude is altered by ten percent. At a six percent increase in ozone magnitude, positive feedbacks prevail, extending the period by roughly 2%. Subsequent research might provide a better look at ozone magnitude influences, using more runs at smaller ozone magnitude increments to determine at what point positive or negative feedbacks prevail on the period of the QBO.

Comparison	Period Δ (years)	Westerly Δ (m/s)	Easterly Δ (m/s)
(O_3 low → super-recovery)	-0.0001 (negligible)	+0.01968	+0.38516
(1980 O_3 → super-recovery)	+0.0403 (≈15 days)	+0.00732	+0.23707

Figure 6. Chart comparison on period length and magnitude of eastery and westerly winds.

Magnitude winds are determined numerically using the same 26km winds. A command is used to locate the maximum (westerly) and minimum (easterly) values. Results show very little change in westerly magnitudes. All runs have maximum westerly values that fall in the 26 meter per second (m/s) range. An examination of the easterly winds shows very little variation as well but comparatively more than the westerlies. The greatest change is noticed between ozone low levels compared to the super-recovery levels with a little more than a 0.01% increase in magnitude.

Conclusion

This research examines the impacts of increased stratospheric ozone levels on the QBO. A particular focus is placed on period changes as well as magnitude winds for both westerly and easterly winds. As expected, the period is extended, but only when comparing the 1980 ozone level run with the super-recovery ozone level run. Wind magnitude increase is also verified but only by fractions of a percent.

While stratospheric ozone does play an important role in the radiative budgets of Earth, real concentration variations do not greatly impact the period, nor magnitude winds of the QBO. Further research is encouraged to examine the influences of photochemical and temperate changes as they can alter ozone concentrations more realistically. Analysis of feedbacks can also be looked at in future research as it is observed that an increase in stratospheric ozone magnitude is not directly related to period change.

Acknowledgements

A special thanks to staff and colleagues at the Department of Meteorology and Climate Science at San Jose State University.

References

Nathan, T., E. Cordero (1994): title. Journal, **21,** pages

Nathan, T., E. Cordero (1994): Ozone Heating and the Destabilization of Traveling Waves during Summer. Geophysical Research Letters, **21,** 1531-1534.

Cordero, E., T. Nathan, R. Echols (1997): An Analytical Study of Ozone Feedbacks on Kelvin and Rossby-Gravity Waves: Effects on QBO. Journal of the Atmospheric Sciences, **55,** 1051-1062.

Cordero, E., T. Nathan (2000): The Influence of Wave- and Wave Mean- Ozone Feedbacks on the Quasi-biennial Oscillation. Journal of the Atmospheric Sciences, **57,** 3426-3442.

Nathan, T., E. Cordero (2007): An Ozone-Modified Refractive Index for Vertically Propagating Planetary Waves. Journal of Geophysical Research, **112,** 1-12.

McCormack, J., T. Nathan, E. Cordero (2010): The Effect of Zonally Asymmetric Ozone Heating on the Northern Hemisphere Winter Polar Stratosphere. Geophysical Research Letters, **38,** 1-5.

Grogan, D., T. Nathan, R. Echols, E. Cordero (2012): A Parameterization for the Effects of Ozone on the Wave Driving Exerted by Equatorial Waves in the Stratosphere. Journal of the Atmospheric Sciences, **69,** 3715-3731.

Autin, J., J. Wilson (2006): Ensemble Simulations of the Decline and Recovery of Stratospheric Ozone. Journal of Geophysical Research, **111**, 1-16.

Li, F., R. Stolarski, P. Newman (2008): Stratospheric Ozone in the Post-CFC Era. NASA, 1-14.

Student who received 'A' in Metr 240

Numerical Simulations on the Synoptic Conditions Surrounding the Valley Fire

Introduction

The Valley Fire was ignited during the afternoon of 12 Sep 2015 around 13:21 PDT. The fire grew to roughly 100 acres within an hour, and began spotting. The fire continued to grow at a steady rate until 15:00 PDT, at which point strong northwesterly flow developed over Lake County. The strong northwesterly flow titled the convective plume, increasing the amount of spotting and rate of spread of the fire. The fire remained active through the night, and burned over 40,000 acres by the morning of 13 Sep 2015. In addition, the fire destroyed over 2000 structures, injured four firefighters, and killed four civilians. The final perimeter of the Valley Fire is shown in Fig 1. As the Valley Fire is one of California's most destructive fires, it is vital to understand the atmospheric dynamics that contributed to rapid growth of this conflagration.

Preliminary analysis on the meteorological conditions surrounding the Valley Fire suggests a strong influence from tropical moisture. In the days preceding the incident, Hurricane Linda was located along the coast of Baja California. The mid-level moisture associated with Linda was advected northward as the hurricane's circulation decayed. As the moisture moved northward, precipitation developed along the Californian coast. Due to the dry air near the surface, the majority of the precipitation fell as virga. The evaporative cooling associated with the virga likely formed a meso-high (Nachamkin, McAnelly, and Cotton 1994) directly off the Bay Area coast, which was particularly noticeable at the 850hPa level. The 850hPa geopotential height gradient tightened over Lake County with the formation of the meso-high, which in turn increased the strength of the northwesterly flow. The goal of this

numerical study is to further determine the influence tropical moisture had on the development of the strong northwesterly flow over Lake County.

Model Setup

The Weather Research and Forecasting model ARW core (WRF-ARW) was used to simulate the atmosphere during the Valley Fire. The model consists of four domains in total, three of which are nested using basic nesting (Fig 2). The outermost domain is 1890x1755km^2, with a horizontal grid spacing of 27km. The two intermediate domains are 1089x1089km^2 and 750x750km^2, with horizontal grid resolutions of 9km and 3km, respectively. The innermost domain is 115x109km^2 with a horizontal grid resolution of 1km. Each domain has the same number of vertical levels, with 30 terrain following sigma levels that span from the surface to 50hPa.

A range of physics parameterizations were used in WRF for the simulations. The parameterization schemes used for the longwave and shortwave radiation budget are the RRTM scheme (Mlawer et al. 1997) and the MM5 shortwave scheme adapted by Dudhia (1989). The YSU planetary boundary layer scheme developed by Hong, Noh, and Dudhia (2006) was used. The surface layer used is based off the MM5 scheme, which relies on using stability functions to compute the surface momentum, moisture, and heat exchange coefficients (Dyer and Hicks, 1970; Paulson, 1970; Webb, 1970). The single moment 3-class microphysics scheme from Hong, Dudhia and Chen (2004) was used. These parameterizations did not vary throughout each domain. The only parameterization that did vary in-between the domains was the Kain-Fritsch cumulus parameterization scheme (Kain 2004). The cumulus parameterization

scheme is enabled for the outermost domain and the coarser intermediate domain, and is disabled for the finer intermediate domain and innermost domain.

In order to fully understand the impacts of the tropical moisture on the Valley Fire, two simulations are conducted. The first simulation uses the parameterizations as previously discussed in order to determine the model's ability to replicate the observed conditions. In the following run, the microphysics and cumulus parameterizations are disabled in order to eliminate any precipitation effects.

The 0.25° Global Forecasting System (GFS) provides the initial and boundary conditions for the two simulations. The boundary conditions update in six hour increments using the 0000, 0600, 1200, 1800 UTC GFS zero-hour forecast. Both simulations are initialized as a cold-start at 11 Sep 2015 UTC, and run for a period of 72 hours. The outermost and coarser intermediate domains record every three and two hours, respectively. The finer intermediate domain and innermost domain record every thirty minutes, in order to better capture the evolution of the winds near the surface.

Results

The analysis of the simulations focuses on the finer intermediate domain and the innermost domain. Due to the small domain size of the innermost domain, the domain is unable to capture any precipitation along the coast of California nor the formation of the meso-high. As a result, the finer intermediate domain will be used to analyze how precipitation effects influence the meso-high. Comparisons to surface remote automated weather stations (RAWS) are based off the innermost domain.

The total accumulated precipitation for the first simulation is shown in Fig 3. The total accumulated precipitation shows the majority of measureable precipitation occurred off the coast of northern California. Light accumulations are observed west of San Francisco, but virtually no precipitation made it to the surface inland over the coastal mountain ranges, which suggests nearly any precipitation over land fell as virga. The simulated maximum reflectivity (which is analogous to composite reflectivity) and precipitation tendency fields further support this claim. The simulated maximum reflectivity (hereafter SMR) field shows a main band of precipitation moving northward along the Californian coast starting at 12 Sep 2015 11:00 UTC. As the band of precipitation moved northward, the majority of the precipitation evaporated before making to the surface, both over land and sea. This is evident when comparing the SMR field to the precipitation tendency field (Fig 4).

The impact of the virga is clearly seen when comparing the SMR to the 850hPa geopotential heights. At 13 Sep 2015 00:00 UTC, the majority of the virga was falling to the southwest of San Francisco. Superimposing the SMR over the 850hPa heights shows a meso-high located under the region with strongest returns (Fig 5). The location of the meso-high substantially increased the height gradient over the greater Lake County area when compared to 12 hours earlier (Fig 6), helping to generate the strong northwesterly flow over the area.

Disabling the microphysics and cumulus parameterization schemes in the following simulation prevented any precipitation from developing within the domains. Difference plots between the two simulations show what influence the precipitation effects had on the synoptic evolution. When comparing the 850hPa geopotential heights between the two simulations, a noticeable height anomaly is observed off the coast of the Bay Area around 13 Sep 2015 00:00

UTC (Fig 7). The 850hPa heights are up 15m higher in the simulation with precipitation enabled compared to when precipitation disabled, implying the meso-high does not form without the virga.

The 850hPa height gradient decreases over and along the central Californian coast without the formation of the meso-high. This is evident when comparing the 850hPa heights of the two simulations at 13 Sep 2015 00:00 UTC (Fig 8). The 850hPa winds decreased up to $8ms^{1}$ over the greater Lake County area (Fig 9), which is expected with a lesser height gradient. While the wind speeds decrease, the northwesterly flow was still present in the simulation with no precipitation. The decrease in wind speeds are not only observed aloft, but at the surface as well.

The surface winds of the two simulations were compared to observed winds at the Konocti RAWS. The Konocti RAWS is located roughly 5 miles to the northwest of the Valley Fire incident. In order to compare the model to the Konocti RAWS, a $1km^2$ average was made using the closest grid points surrounding the location on the RAWS. Figure 10 shows the comparison of the WRF 10m wind speed and direction to the observed wind speed, direction, and gusts. The two WRF simulations were close to one another in terms of wind speed and direction, but overestimated the strength of the surface wind. The error between WRF and the observed conditions is likely the result of the cold-start initialization. The two simulations began to noticeably diverge around 11 Sep 2015 23:00 UTC (16:00 PDT). Around this time, the WRF simulation with no precipitation consistently produced weaker wind speeds compared to the observed winds and the other WRF simulation.

The WRF simulation with precipitation replicated the observed conditions fairly well until the onset of strong surface winds. The observed surface winds experienced a lull around 16:00 UTC on 11 Sep 2015. After the lull, the observed sustained winds quickly increased in strength, peaking at 10.7ms^{-1} around 00:00 UTC on 13 Sep. The WRF simulation with precipitation failed to capture the intense surface winds, and underestimated the maximum sustained wind speed by 3ms^{-1}. In addition, the peak winds lagged behind the observations by three hours. While the simulation experienced difficulty predicting the surface wind magnitude and timing, the simulation managed to capture the overall pattern. In the simulation with no precipitation, the 10m winds behaved similar to the simulation with precipitation, but were weaker in comparison. The peak winds in the simulation without precipitation were 3ms^{-1} slower than the peak winds in the simulation with precipitation.

Conclusions and Discussion

Two simulations in WRF were conducted to determine the influence of tropical moisture on the Valley Fire. The first simulation included the impact of precipitation effects, whereas the second simulation disabled precipitation forming in the domain and therefore eliminating any precipitation effects. A comparison between the two simulations reveals the extensive virga and evaporative cooling off the Californian coast led to the development of a meso-high. The meso-high tightened the height gradient over the greater Lake County area, which lead to the development of strong northwesterly flow. When precipitation effects are disabled, the meso-high does not form, leading to weaker a height gradient and northwesterly flow. The next step in analyzing this case is to use HYSPLIT in order to verify the tropical origin of the moisture that resulted in the widespread virga.

Comparisons of the 10m winds from the WRF simulations to observed surface winds show that WRF managed to capture the overall trend of the surface winds. While the overall trend is captured, the model experienced difficulty with the timing and strength of the peak winds. When precipitation effects are disabled, the peak surface winds decrease by $3ms^{-1}$ compared to when precipitation effects are enabled. As the 10m winds are dependent on the PBL parameterization scheme, comparing the surface observations to the 925hPa level may provide slightly more accurate results. If the 925hPa winds also fail to capture the intense surface winds, the spike in the observed winds and gusts may be the result of a mesoscale circulation developing over the region as the result of the fire interacting with the atmosphere. Further simulations are required to test this hypothesis.

Fig 7: The location and final fire perimeter of the Valley Fire. The red dot indicates the location of the Konocti RAWS

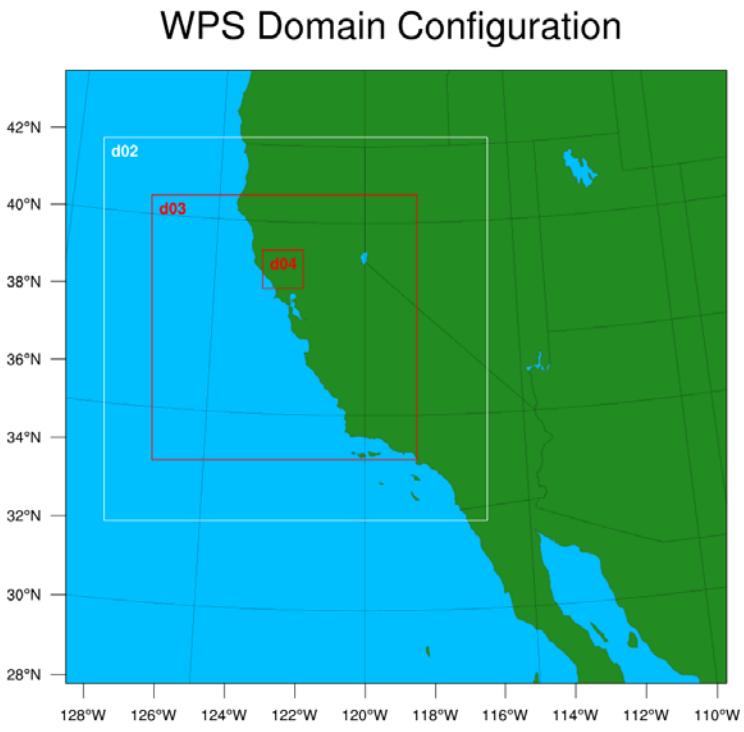

Fig 8: Map of the domains used

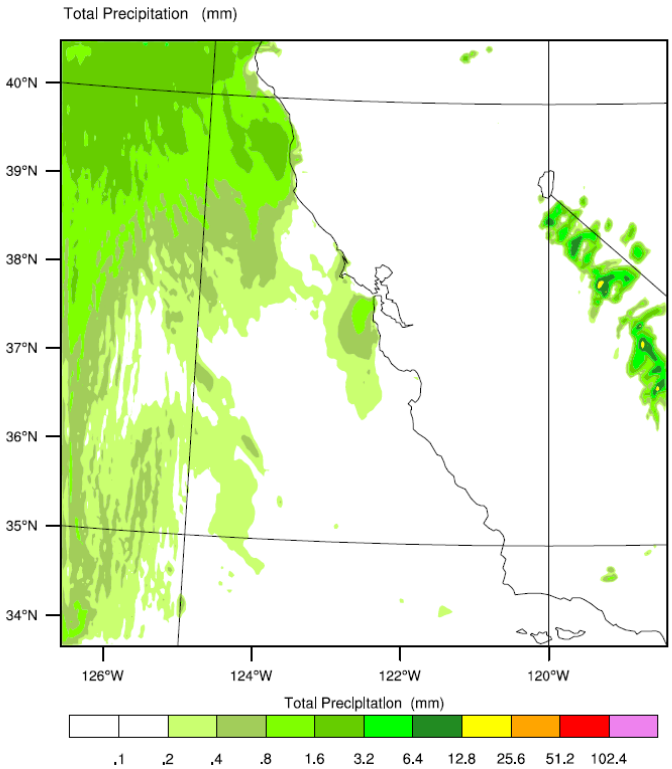

Fig 3: The total accumulated precipitation from 00:00 UTC 11 Sep 2015 - 00:00 UTC 14 Sep 2015

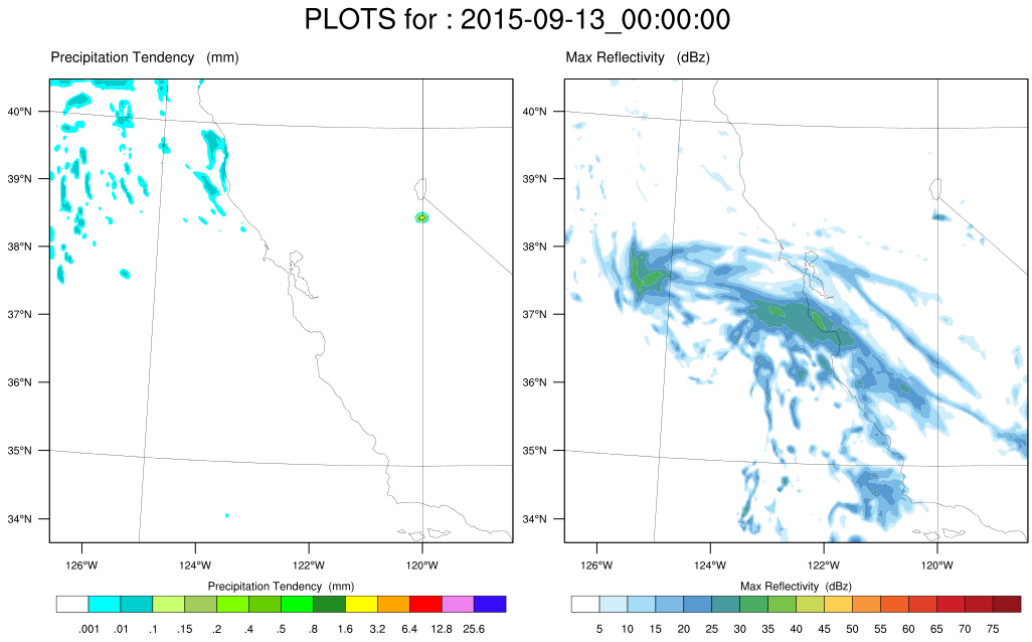

Fig 4: The precipitation tendency and the maximum reflectivity at 00:00 UTC 13 Sep 2015

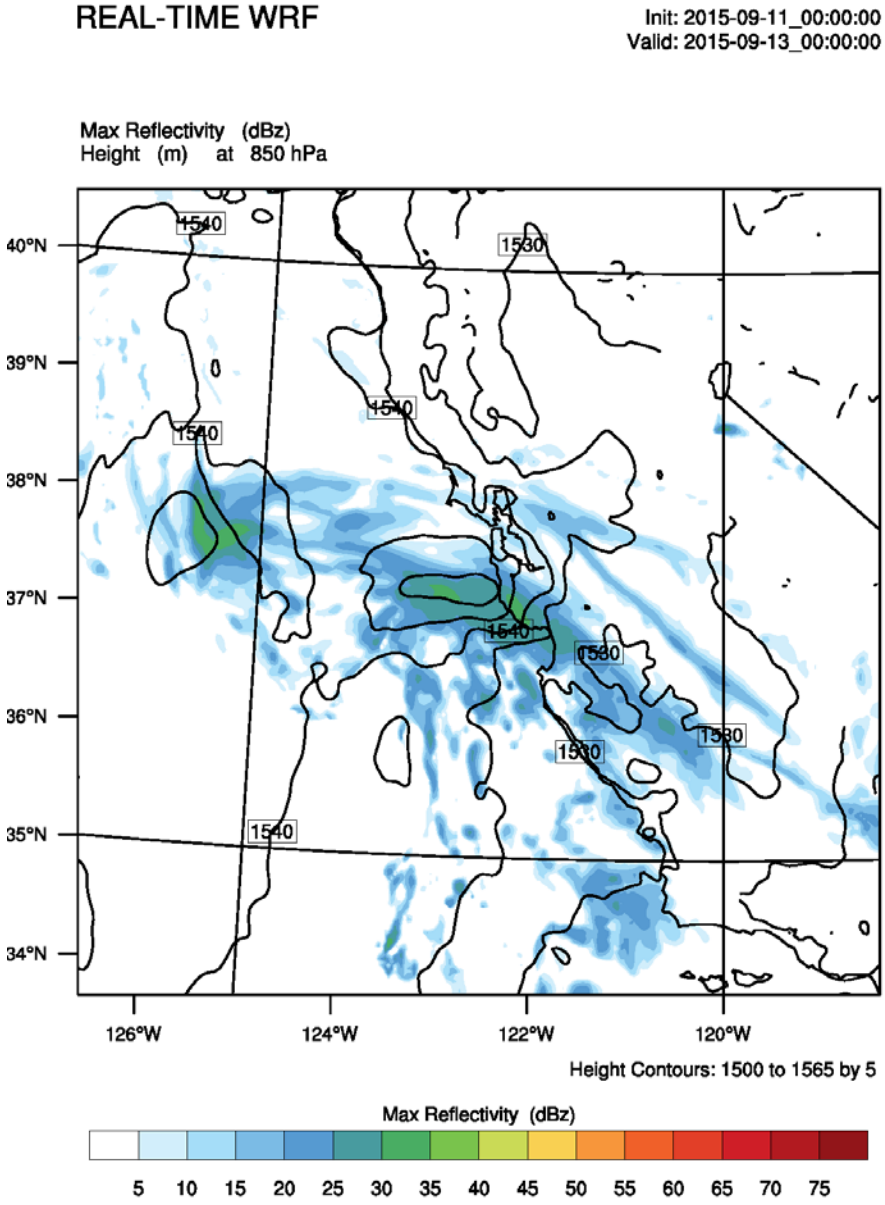

Fig 5: The maximum reflectivity superimposed over the 850hPa geopotential heights

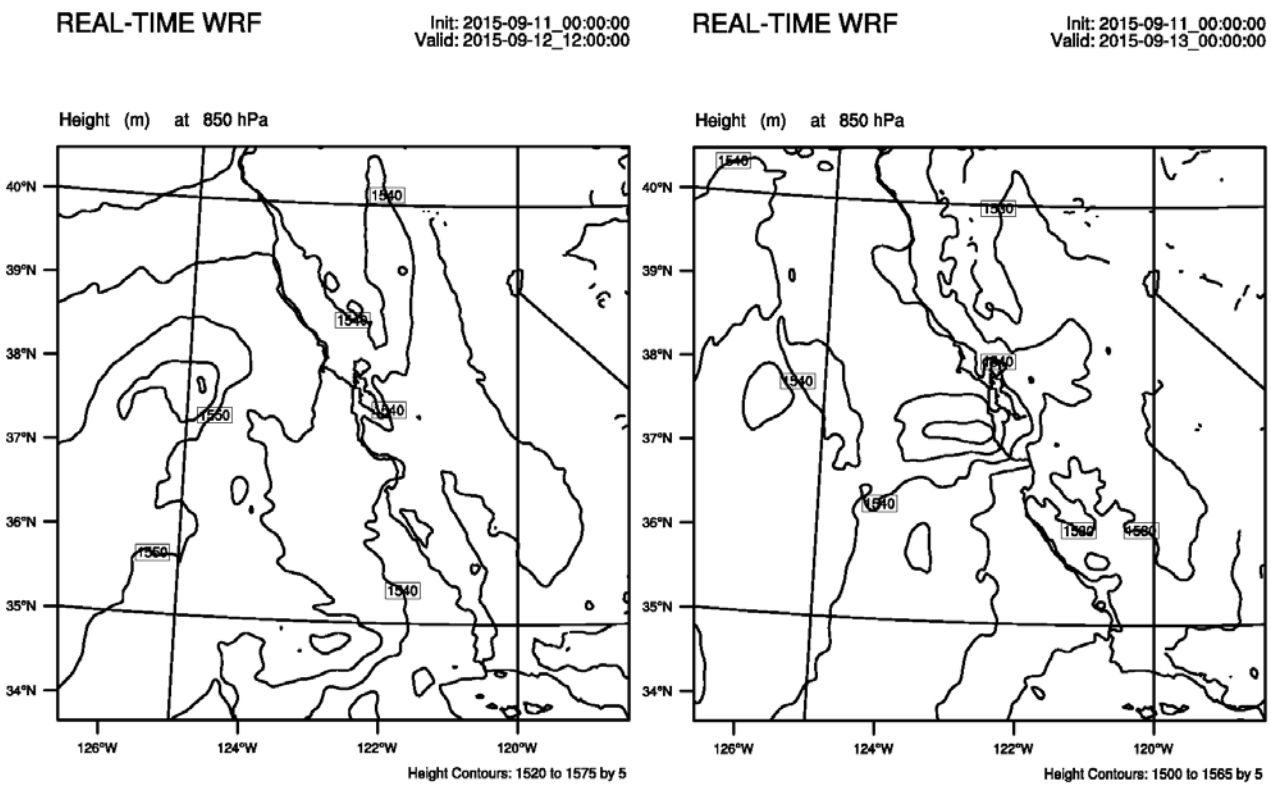

Fig 6: A comparison of the 850hPa geopotential heights at 12:00 UTC 12 Sep 2015 and 00:00 UTC 13 Sep 2015

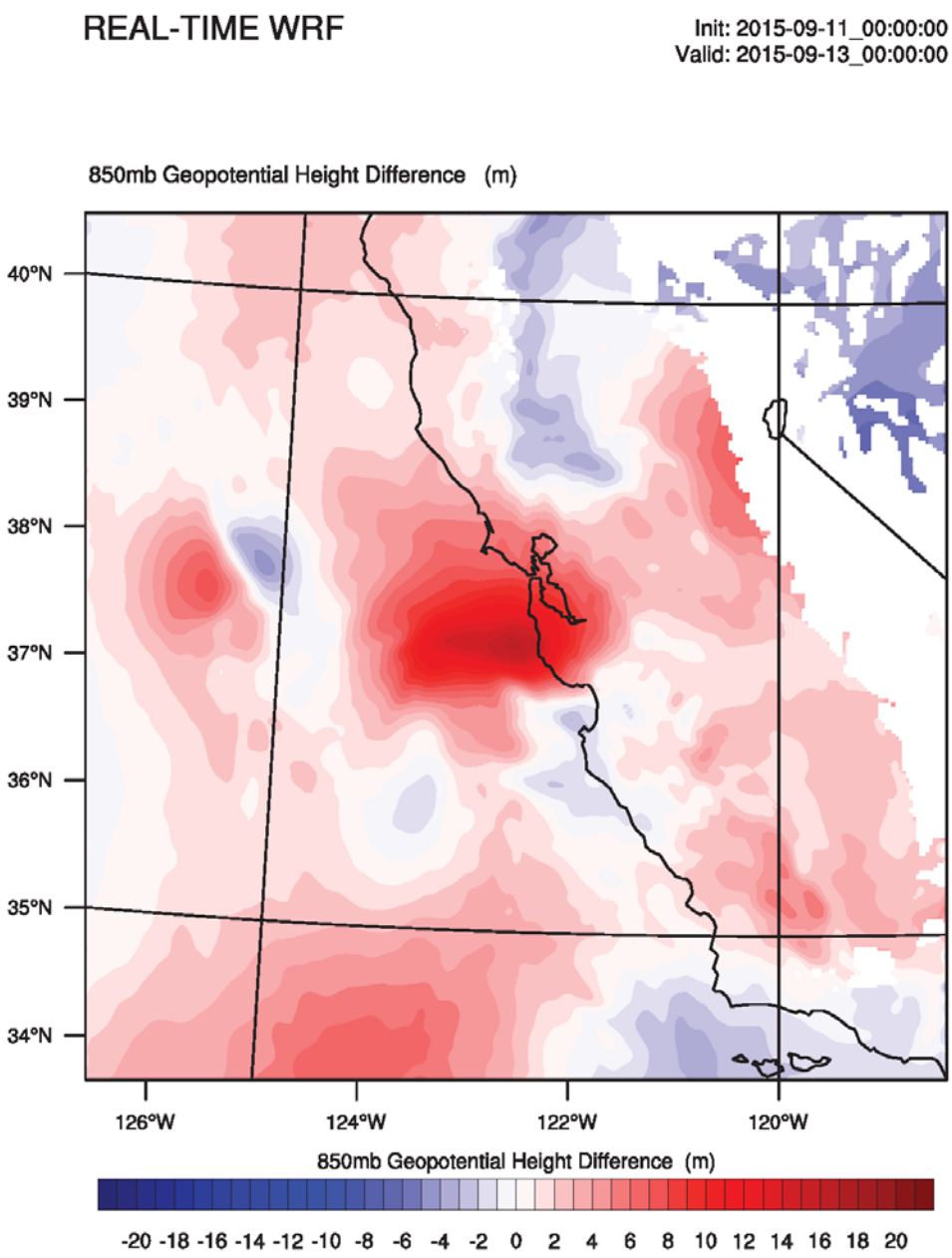

Fig 7: Difference between the 850hPa geopotential heights at 00:00 UTC 13 Sep 2015

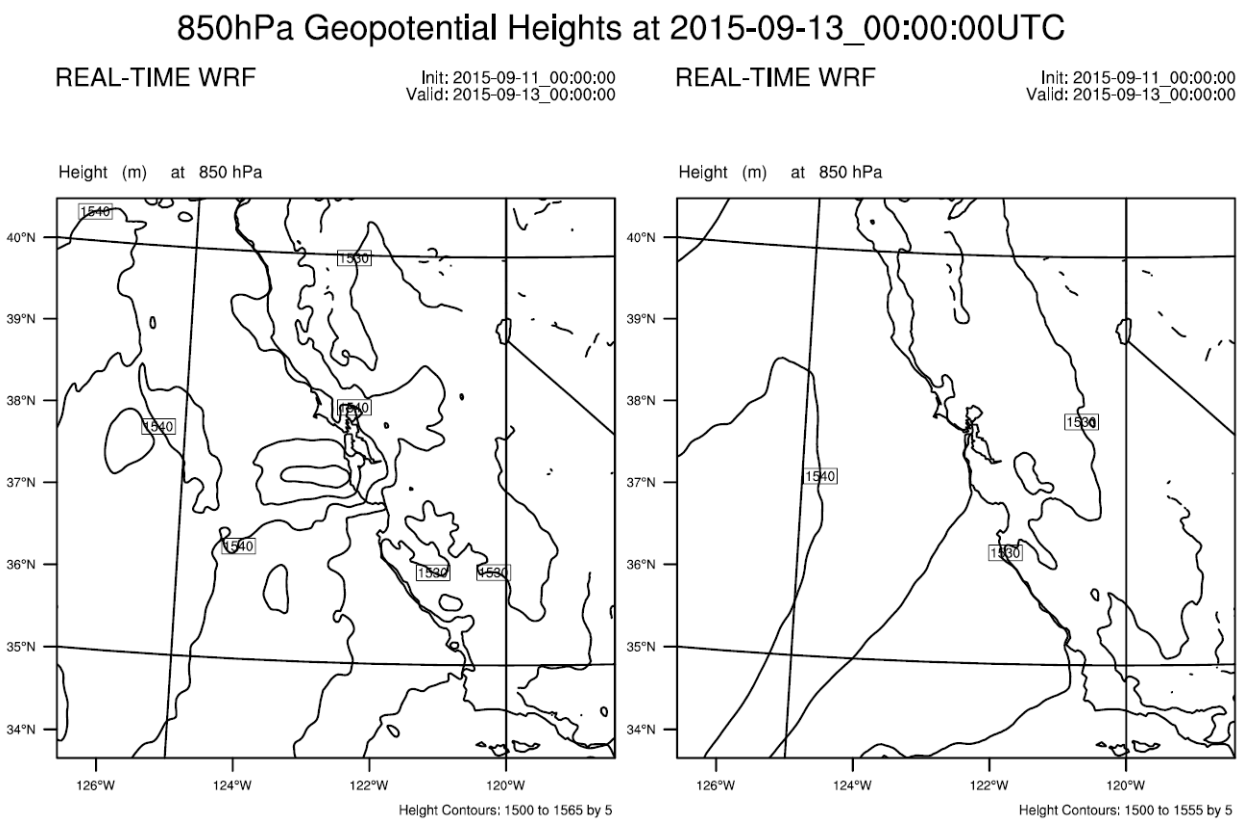

Fig 8: Comparison between the 850hPa geopotential heights at 00:00 UTC 13 Sep 2015. The image on the left is the WRF simulation with precipitation, and the image on the right is the WRF simulation with no precipitation.

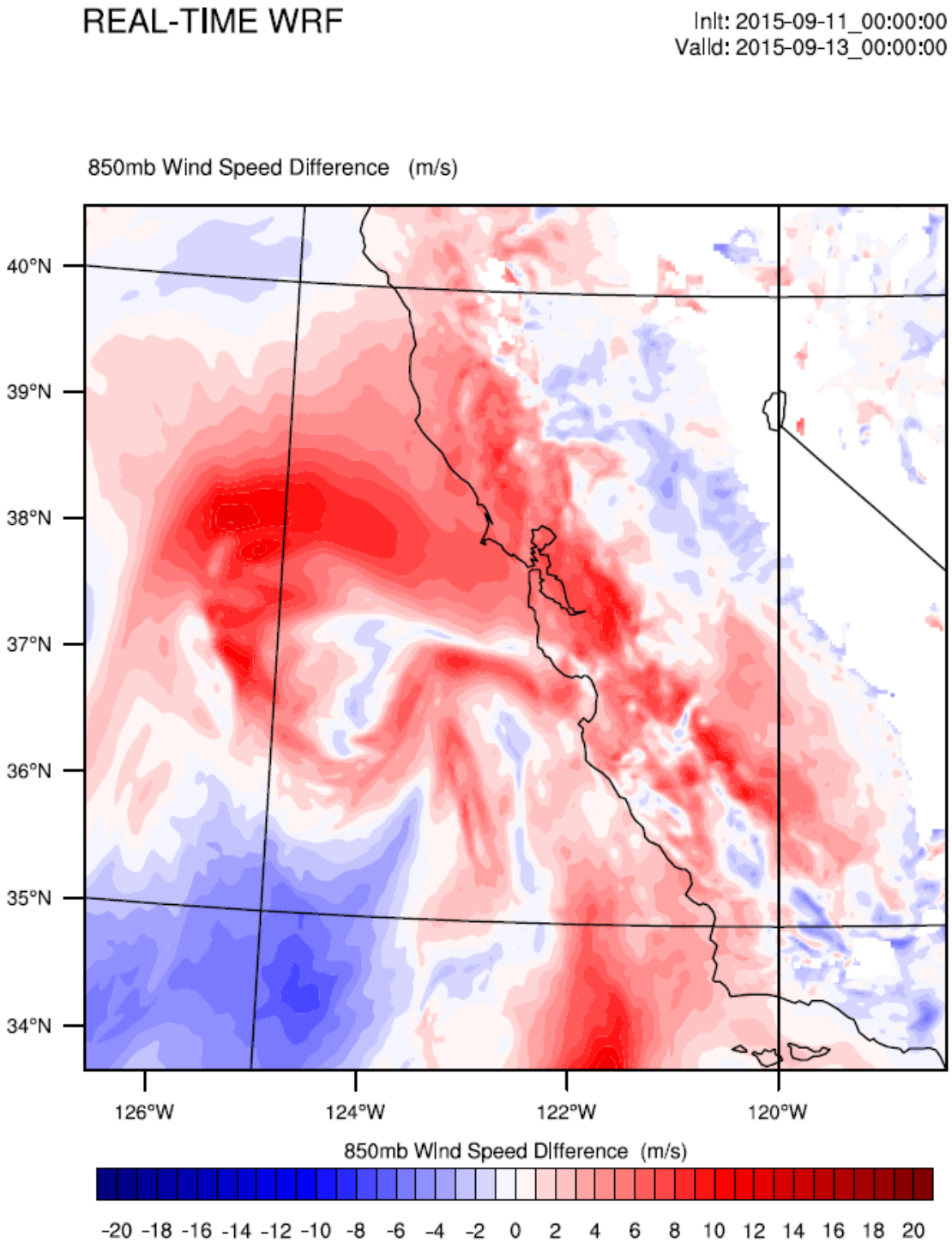

Fig 9: Difference between the 850hPa wind speeds at 00:00 UTC 13 Sep 2015

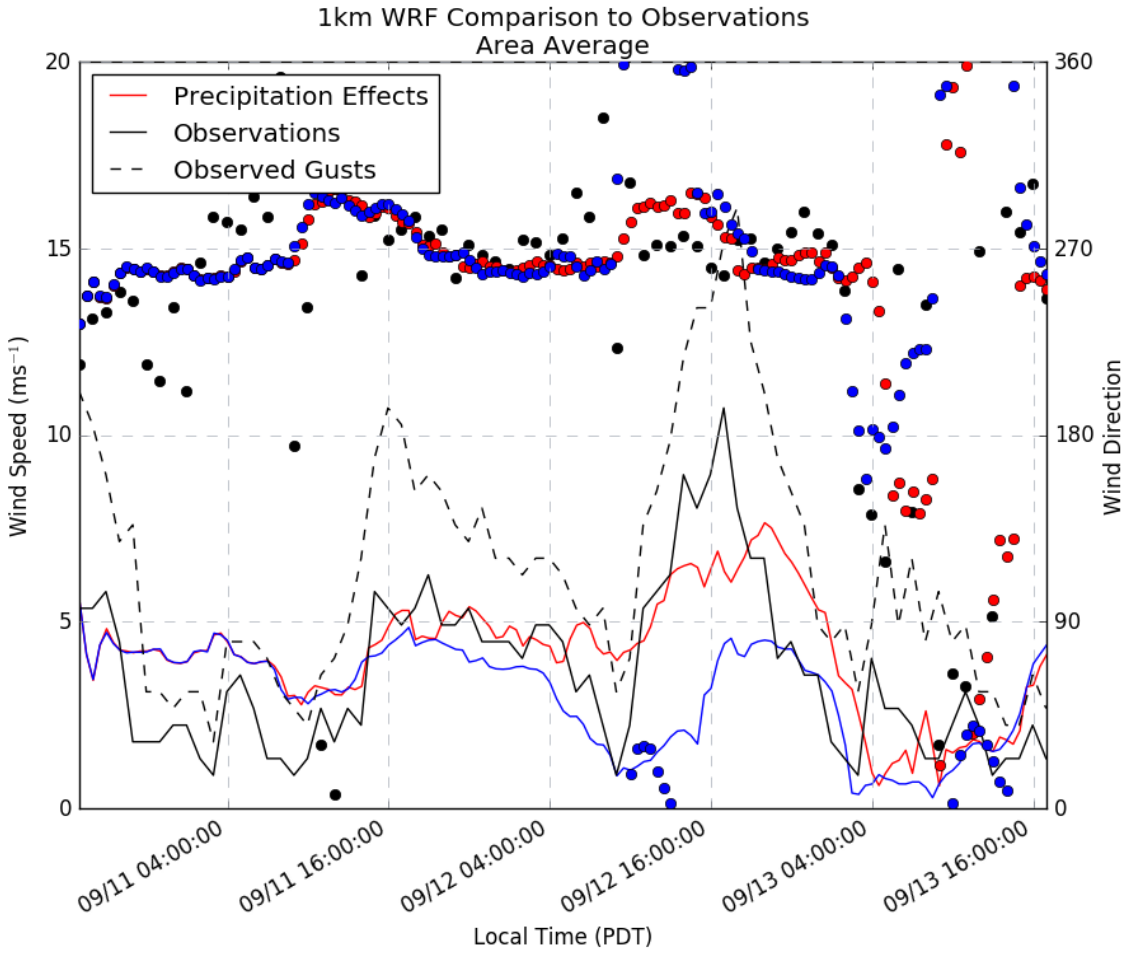

Fig 10: WRF 10m winds compared to the observed winds at Konocti RAWS

References

Dudhia, J. (1989). Numerical study of convection observed during the winter monsoon experiment using a mesoscale two-dimensional model. *Journal of the Atmospheric Sciences*, *46*(20), 3077-3107.

Dyer, A. J., & Hicks, B. B. (1970). Flux-gradient relationships in the constant flux layer. *Quarterly Journal of the Royal Meteorological Society*, *96*(410), 715-721.

Hong, S. Y., Noh, Y., & Dudhia, J. (2006). A new vertical diffusion package with an explicit treatment of entrainment processes. *Monthly Weather Review*, *134*(9), 2318-2341.

Kain, J. S. (2004). The Kain-Fritsch convective parameterization: an update. *Journal of Applied Meteorology*, *43*(1), 170-181.

Mlawer, E. J., Taubman, S. J., Brown, P. D., Iacono, M. J., & Clough, S. A. (1997). Radiative transfer for inhomogeneous atmospheres: RRTM, a validated correlated-k model for the longwave. *Journal of Geophysical Research: Atmospheres*, *102*(D14), 16663-16682.

Nachamkin, J. E., McAnelly, R. L., & Cotton, W. R. (1994). An observational analysis of a developing mesoscale convective complex. *Monthly weather review*, *122*(6), 1168-1188.

Paulson, C. A. (1970). The mathematical representation of wind speed and temperature profiles in the unstable atmospheric surface layer. *Journal of Applied Meteorology*, *9*(6), 857-861.

Webb, E. K. (1970). Profile relationships: The log-linear range, and extension to strong stability. *Quarterly Journal of the Royal Meteorological Society*, *96*(407), 67-90.

Student who received ‘B in METR 240

05/20/15
METR 240

Transpacific Transport of Tropospheric Ozone

Abstract:

In order to better understand the transpacific transport of ozone plumes found on the eastern coast of Asia, the WRF-ARW numerical model was applied over a 240-hour time period using GFS-ANL data. The WRF output files were then converted in order to be processed by the HYSPLIT trajectory model. These converted trajectories were compared to real ozone concentrations, measured by weather stations found under their paths. The WRF-converted HYSPLIT trajectories were also plotted and against HYPSLIT trajectories generated from Global Data Assimilation System (GDAS) for the purpose of comparing the patterns of the two trajectories and any corresponding ozone increases. The accuracy of both types of projected trajectories proved inconclusive due to the shortage of ozone data and the lack of any consistent correlation between ozone levels and trajectory paths.

1. Introduction:

Industrialized countries such as the United States of America have made great strides driving down concentrations of anthropogenic ozone over the past decades. This has in turn made it possible for the EPA to set standards and regulate, through the withholding of federal funding and potential lawsuits, as outlined in the Clean Air Act. As of

2015, the EPA has lowered the level of acceptable ozone by 5 ppb to 70 ppb, averaged over an 8-hour period. Consistently high surface ozone concentrations are incredibly harmful to life in general. Over time, high levels of ozone not only have the potential to severely damage the lungs but the USDA found it to be more harmful to crops than all other pollutants combined. For these reasons, it is important that we come to a better understanding as to how and where anthropogenic ozone is produced, and how it affects the areas through which it travels. One area of focus and study is the continent of Asia, with many industrializing countries producing significant amounts of anthropogenic ozone. This study attempts to track spikes in ozone, from the east coast of Asia across the Pacific and beyond, using WRF, a mesoscale numerical model, and HYSPLIT, a hybrid single particle Lagrangian integrated trajectory model.

1.2 Chemistry

Ozone can be produced anthropogenically but ozone is not simply produced; it is the product of a photochemical reaction involving sunlight, NO_x, and volatile organic compounds (VOCs) produced by human activity. Some examples are NO_x, SO_2, and CO from fossil fuels; CH_4 and NMHC produced anthropogenically; NO_x, from biomass burning and soil emissions; and SO_2 from volcanic activity and shipping (Carmichael et. al, 1998). For this reason ozone can continue to be produced in a concentrated cloud of pollutants long after it has left its source. These plumes can travel across the Pacific in 5 to 10 days. (Zhang et al, 2008). Accordingly, the WRF and HYSPLIT models were run for 240 hours or 10 days in order to potentially capture the transpacific route of such a pollution plume.

1.3 Background

Several studies have been conducted with the intention of tracking and documenting the effect of transpacific ozone transport. In one study, anthropogenic Asiatic ozone was found to increase afternoon concentrations of surface ozone in the United States by 4 to 7 ppb (Fiore et al., 2002). In another study focusing on specific areas, no increase in ozone from Asian anthropogenic emissions was noted at Trinidad Head in California, while in Sequoia National Park they observed a 5 to 9 ppb increase in ozone (Hudman et al., 2004). More recent studies show this to be even more pronounced with the continued industrialization of the Asian continent. Observations at Oregon's Mt. Bachelor Observatory indicated a consistent mean increase in ozone resulting from Asian emission by as much as 12 ppb (Zhang et al, 2008). During episodes of strong ozone exceeding 60 ppb in Los Angeles, Asian anthropogenic emissions were found to contribute anywhere from 8 to 16 ppb (Lin et al., 2014). It has become apparent from this sampling of documented studies that the influence ozone and ozone components emitted in Asia is adversely effecting ozone levels in North America. A gradual increase in ozone concentrations attributed to Asian industrialization is also evident. These increases in ozone may seem somewhat trivial and small in number, but when a just a few ppb determine what is in compliance and what is in violation of EPA standards, then every ppb counts.

2. Models and data

For this study, the Weather Research Forecast – Advanced Research WRF (WRF-ARW) mesoscale numerical model and HYSPLIT trajectory model were used. The WRF model can generate atmospheric simulations using real data and is continuously updated with advanced numerical, physical and data assimilation (wrf-model.org). The WRF-ARW

model was set to 15x15km resolution with 30 vertical levels and a domain of the northern Pacific Ocean and the continents bordering it. A 240-hour or 10-day simulation with time intervals of 21600 seconds (6 hours) was used. The time step was 60 seconds.

Real gribbed Global Forecasting System Analysis data (GFS-ANL), with 1 degree resolution and using a model cycle every 6 hours over 10-day periods, was input into the WRF model, following the isolation of a spike in ozone. The WRF model, using this data, then produced wrfout files which were then converted HYSPLIT compatible ARL files to be used to plot trajectories in HYSPLIT. The HYSPLIT trajectory model was also used to plot trajectories using Global Data Assimilation System (GDAS) files. GDAS has a resolution of 1 degree or roughly 111km and was used for a 10-day period following a spike in ozone at a specific location.

The HYSPLIT model is capable of computing air parcel trajectories, how it was used for this study, along with more complex methods of atmospheric transport, dispersion, and deposition. It couples the Langarian approach of moving frames of reference and the Eularian fixed 3-dimensional grid (arl.noaa.gov). With the input of converted wrfout files and GDAS files the HYSPLIT trajectory model was able to plot potential trajectories of high ozone readings in the troposphere.

3. Methods

First, spikes in ozone off the eastern coast of continental Asia were isolated. The weather station at Tateno, Japan, located at 35.05 N 140.13 E, supplied this data. There were three prominent spikes in ozone occurring in late spring during the years of 2008, 2010, 2013. Data was then located for these time periods. GFS-ANL data was used to run the WRF model for 240 hours after the spike in ozone was recorded at Tateno. The

resultant wrfout files were then converted using HYSPLIT's WRF data conversion option, in order to plot trajectories from Tateno. As second set of data, GDAS, which was already HYSPLIT compatible, was then input separately into HYSPLIT in order to plot and compare trajectories. Finally, based on the projected trajectories weather stations with ozone data were located on these trajectory paths in order to investigate corresponding increases in ozone or lack thereof.

4. Results

The HYSPLIT model successfully produced trajectories using both the data converted from the wrfout data as well as from the GDAS data. These trajectories, originating from the same location and derived from "real data," initially followed somewhat similar paths, but often deviated greatly over the 10-day period of the model run. The weather stations with ozone data, of which there were very few located below these trajectories, at times showed increases in ozone which could whimsically be attributed to the ozone increases in the Tateno location many days earlier. However, for the most part, with regard to each potential correlation, there were several instances suggesting the opposite.

4.1 Trial 1 (April 30, 2008)

The first trial attempt to track a sharp rise in lower tropospheric ozone levels (106 ppb) which took place in Tateno, Japan at 1165 m on April 30, 2008. Two HYSPLIT generated trajectories, one with data from WRF and the other using GDAS data, were then projected 240 hours out from the given date and location. Both trajectories take a similar route to the Aleutian Islands over the first 3 days. After the 3rd day the projected

trajectories begin to deviate. The HYPSLIT compatible GDAS data's trajectory reached an elevation of 4000 m and continued on a westward trajectory eventually turning to the south off the west coast of California and terminating at an elevation of 1000 m. The HYSPLIT trajectory generated from WRF data shows that after the 3rd day it reaches an elevation of about 2500 m and then doubles back on its trajectory, effectively turning southward and then westward. This trajectory terminated north east of the GDAS trajectory, off the coast of the Pacific Northwest at an elevation of about 500 m. Neither trajectory passed over any weather stations with ozone data so it wasn't possible to correlate any rise in ozone levels with the ozone concentrations originally recorded in Tateno.

4.1 Trial 2 (May 12, 2010)

The second trial attempts to track two spikes in ozone at different elevation, one in the mid troposphere (291 ppb) and another around the tropopause (598 ppb) over Tateno, Japan on May 12, 2010.

The trajectories plotted for the mid troposphere, 6.6 km, differ greatly. The HYSPLIT compatible GDAS data plotted a trajectory that traveled a relatively short distance terminating in the mid Pacific at an elevation around 4.5 km. The HYSPLIT trajectory generated from WRF data on the other had travels over Canada and terminates in the mid Atlantic at an elevation of around 7 km. This trajectory did pass over a weather station located on the western shore of Hudson Bay in Churchill, Canada. It would have passed over Churchill on May 19 at about 8 km elevation but according to their readings there was no noticeable spike in ozone levels in their data.

The trajectories from the ozone spike at the tropopause, unlike those projected for

the mid troposphere, follow very similar paths until after they cross the Atlantic. Both GDAS and WRF generated HYSPLIT trajectories pass over an observatory on the southeastern coast of Ireland at Valentia on May 19th. Readings from the Valentia Observatory show now noticeable spike in ozone levels.

4.1 Trial 3 (May 13, 2013)

The third and final trial attempts to track two spikes in ozone at different elevations. The first was located in the mid troposphere (214 ppb) and the second in the upper troposphere (309 ppb) over Tateno, Japan on May 1, 2013.

The trajectories plotted for the mid troposphere, 5.8 km, as in trial 2, differ greatly. The HYSPLIT compatible GDAS data plotted a trajectory that loops around and winds up terminating northeast of Hawaii below 4km. While the WRF generated HYSPLIT trajectory travels all the way to Europe and terminates at an elevation of 8.5 km. This WRF generated trajectory passed over two weather stations with mixed results. It passed over Churchill, Canada on May 8th at an elevation around 7.5 km. It can be seen here in the ozone data from the Churchill station there is an increase in ozone levels occurring at the elevation specified by HYPSLIT. The causality of this occurrence is debatable but there is definitely a rise in ozone as might be expected given the trajectory. The trajectory from the WRF generated data terminates in the north Atlantic by a weather station located on the Scottish island of Lerwick but there does not appear to be any corresponding increase of ozone levels on or around these days.

The trajectories of the ozone spikes observed in the upper troposphere, around 8km, followed similar paths. The WRF generated data produced a trajectory which crossed the Pacific and the northern United States then doubled back terminating off the west coast at

6.5 km. This trajectory unfortunately did not pass over any weather stations with ozone data. The HYSPLIT compatible GDAS data produced a trajectory which crossed the Pacific and then spiraled southward from Canada into the Pacific Northwest eventually terminating at around 7.5 km. This trajectory passed over Kelowna, British Columbia on May 8th at 8.5 km but the Kelowna station did not record any noticeable increase in ozone the specified elevation.

5. Conclusion

The results were, if not fruitful, at the very least interesting and informative. The fact that very different trajectories can result from "real data" is an interesting phenomenon worth further inquiry. Expanding this project to involve WRF-HYSPLIT Inline as well as WRF-CHEM would certainly improve it. Utilizing some other plotting capabilities of HYSPLIT such as backward trajectories and dispersion would also further this study. Finally, there was a noticeable lack of regularly measured ozone levels so the study currently being conducted in Bodega Bay[1] will, in a small way, contribute to ameliorating this dearth of ozone data.

[1] Our first sounding at Bodega Bay from May 16, 2016 is the final attached figure.

References

Carmichael, R., & Phadnis, J. (1998). Tropospheric ozone production and transport in the springtime in east Asia Gregory Itsushi Zhang ,: and Young Sunwoo, *103*(97).

Fiore, A. M., Oberman, J. T., Lin, M. Y., Zhang, L., Clifton, O. E., Jacob, D. J., … Milly, G. P. (2014). Estimating North American background ozone in U . S . surface air with two independent global models : Variability , uncertainties , and recommendations. *Atmospheric Environment*, *96*, 284–300. http://doi.org/10.1016/j.atmosenv.2014.07.045

Fiore, A. M., Jacob, D. J., Bey, I., Yantosca, R. M., Field, B. D., Fusco, A. C., & Wilkinson, J. G. (2002). Background ozone over the United States in summer : Origin , trend , and contribution to pollution episodes, *107*.

Lin, M., Fiore, A. M., Horowitz, L. W., Cooper, O. R., Naik, V., Holloway, J., … Wyman, B. (2012). Transport of Asian ozone pollution into surface air over the western United States in spring, *117*, 1–20. http://doi.org/10.1029/2011JD016961

Park, R. J., Fehsenfeld, F., & Production, O. (2016). Ozone production in transpacific Asian pollution plumes and implications for ozone air quality in California The Harvard community has made this article openly Please share how this access benefits you . Your story Accessed Citable Link. http://doi.org/10.1029/2004JD004974

Zhang, L., Jacob, D. J., Boersma, K. F., Jaffe, D. A., Olson, J. R., Worden, J. R., … Olson, J. R. (2008). Transpacific transport of ozone pollution and the effect of recent Asian emission increases on air quality in North America : an integrated analysis using satellite , aircraft , ozonesonde , and surface observations.

Trial 1 (4.1)

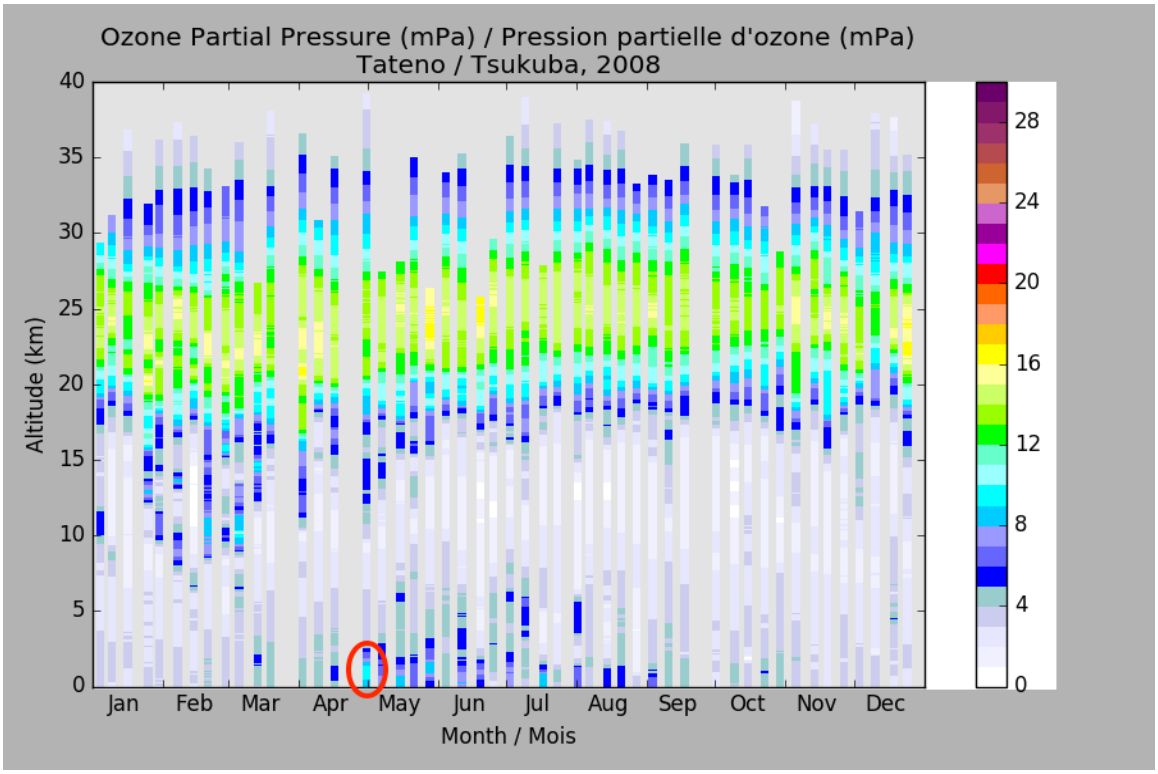
Ozone Partial Pressure (mPa) / Pression partielle d'ozone (mPa)
Tateno / Tsukuba, 2008
Altitude (km)
0
5
10
15
20
25
30
35
40
Jan
Feb
Mar
Apr
May
Jun
Jul
Aug
Sep
Oct
Nov
Dec
Month / Mois
0
4
8
12
16
20
24
28

GDAS

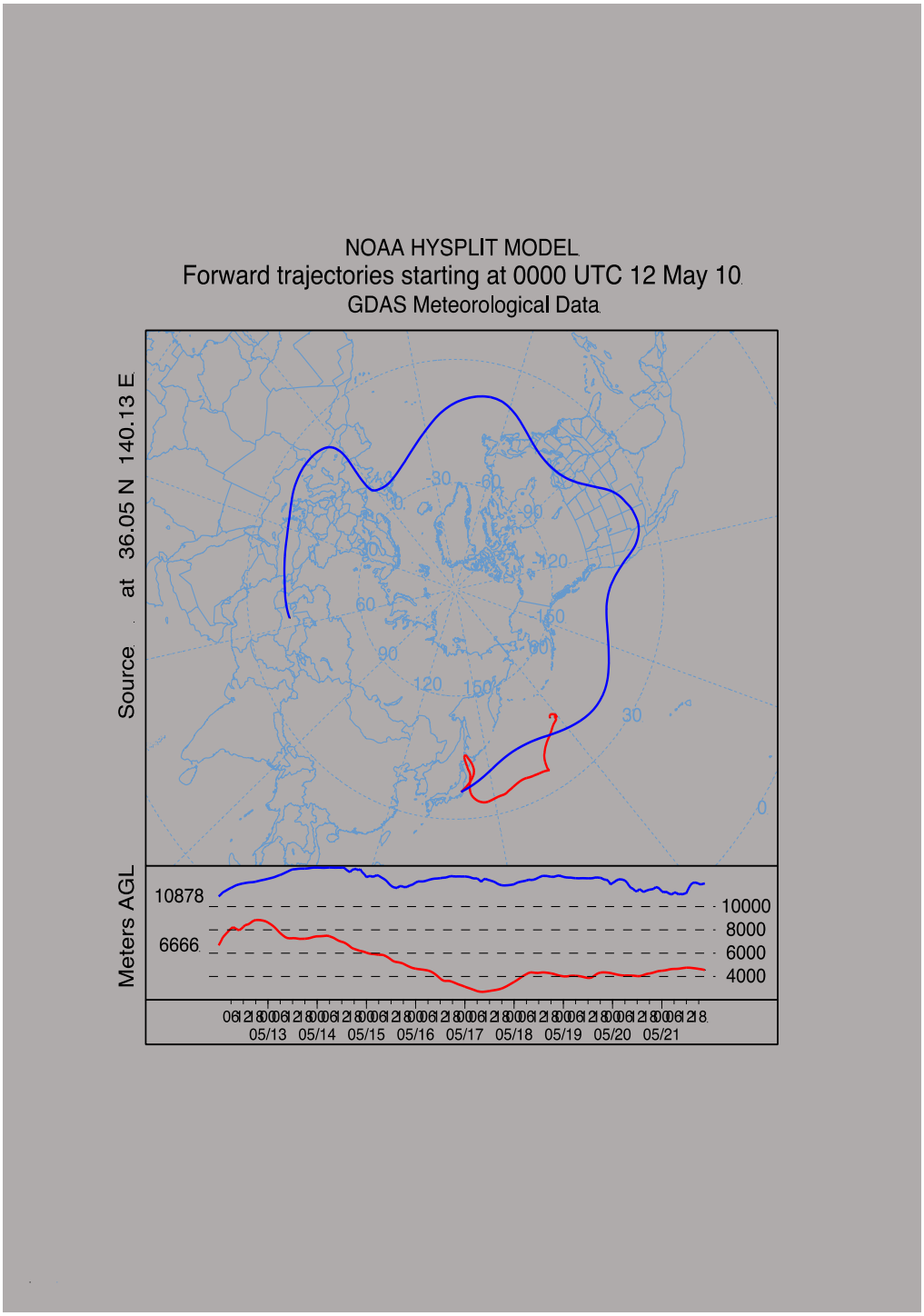
NOAA HYSPLIT MODEL
Forward trajectories starting at 0000 UTC 12 May 10
GDAS Meteorological Data
Source at 36.05 N 140.13 E
Meters AGL
10878
6666
10000
8000
6000
4000
05/13 05/14 05/15 05/16 05/17 05/18 05/19 05/20 05/21

WRF_OUT

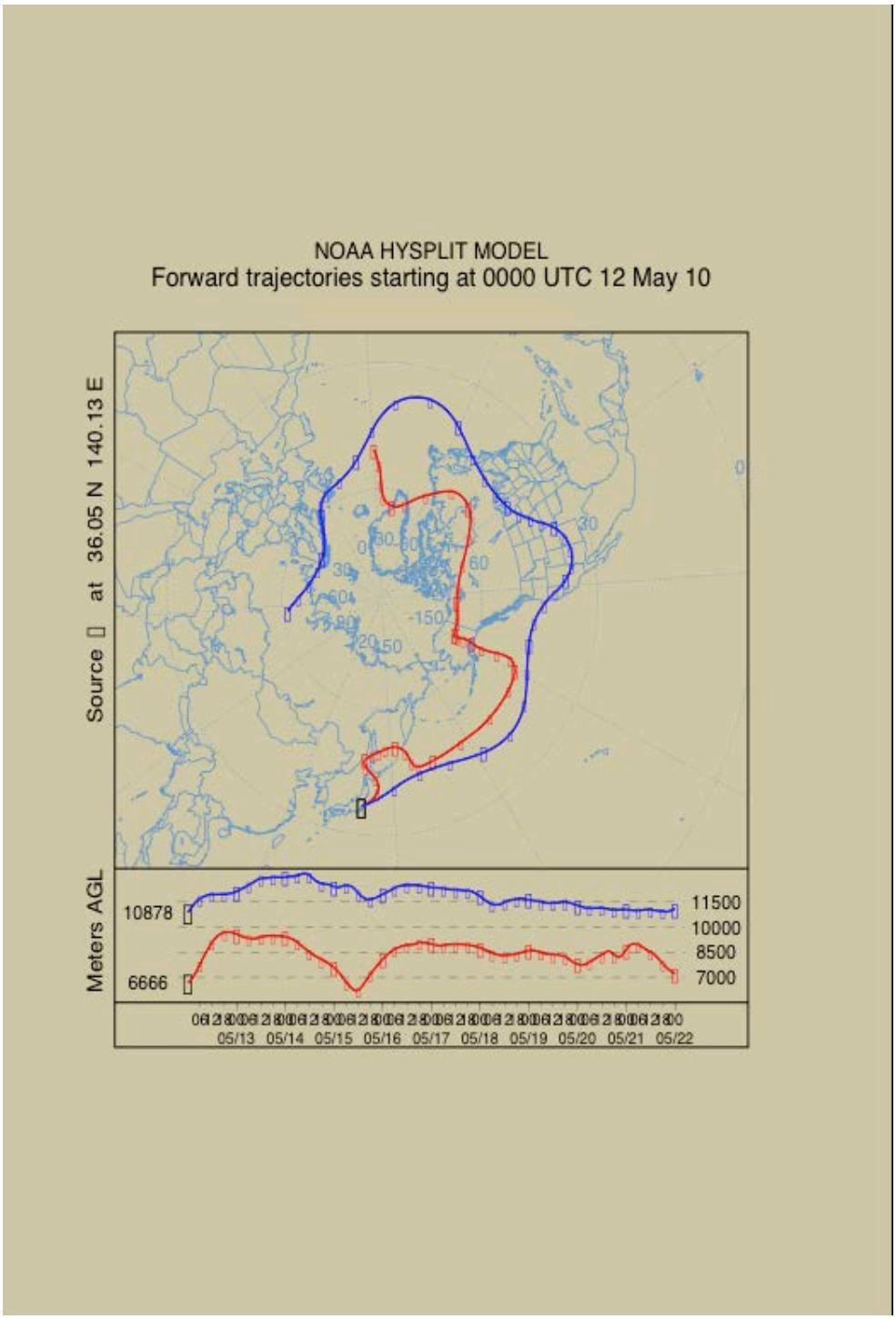
NOAA HYSPLIT MODEL
Forward trajectories starting at 0000 UTC 12 May 10
Source at 36.05 N 140.13 E
Meters AGL
10878
6666
11500
10000
8500
7000
05/13 05/14 05/15 05/16 05/17 05/18 05/19 05/20 05/21 05/22

Trial 2 (4.2)

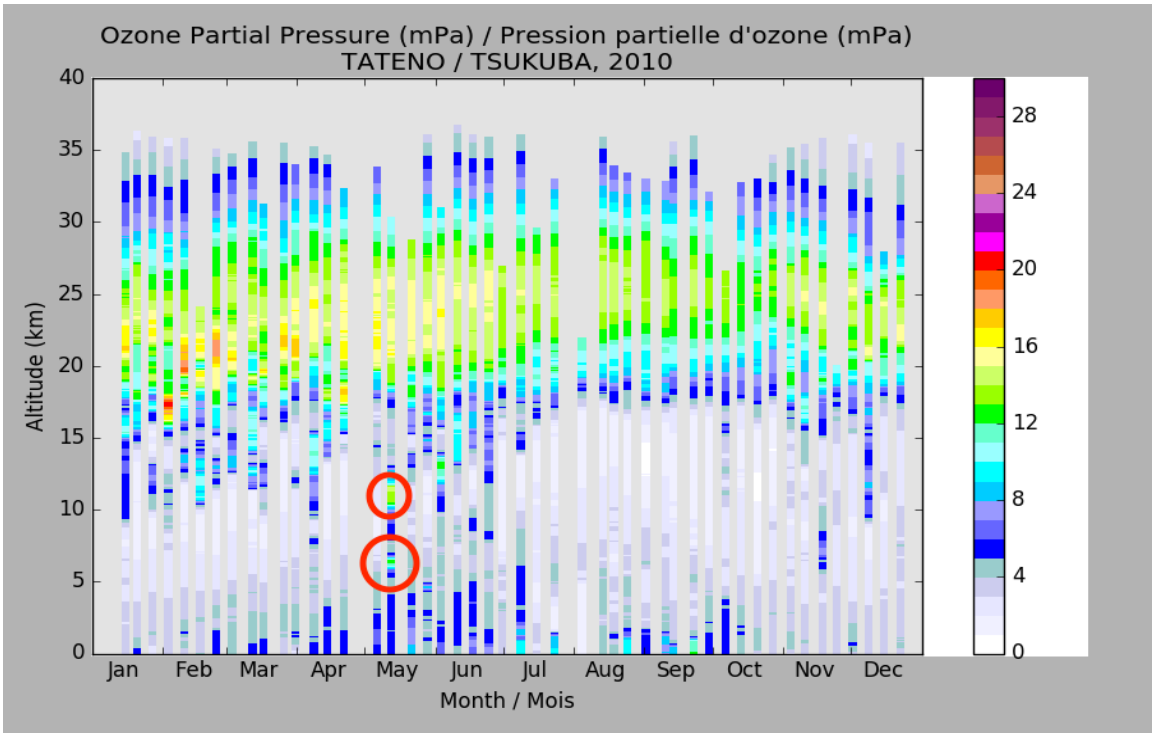
Ozone Partial Pressure (mPa) / Pression partielle d'ozone (mPa)
TATENO / TSUKUBA, 2010
Altitude (km)
0
5
10
15
20
25
30
35
40
Jan
Feb
Mar
Apr
May
Jun
Jul
Aug
Sep
Oct
Nov
Dec
Month / Mois
0
4
8
12
16
20
24
28

GDAS

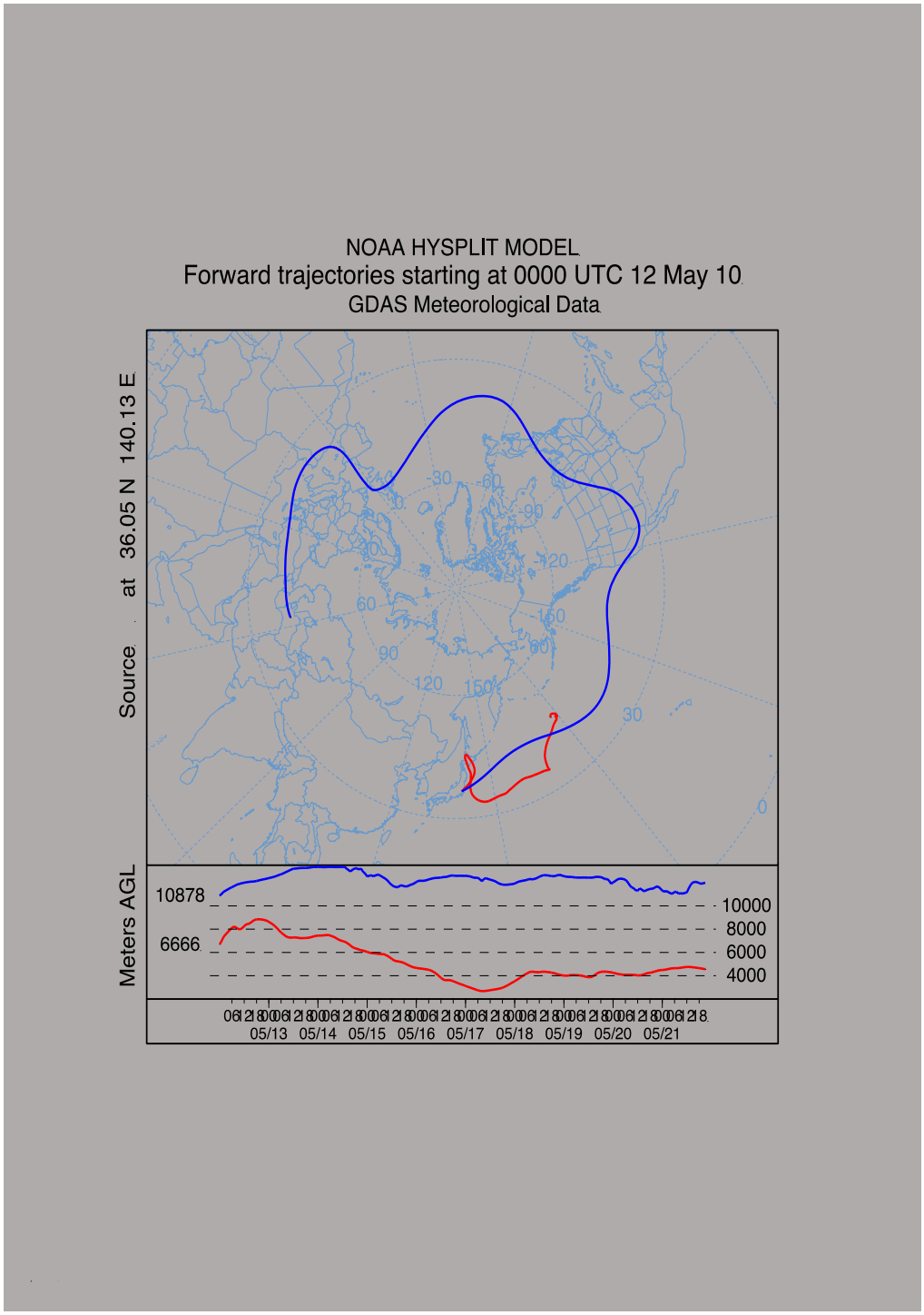
NOAA HYSPLIT MODEL
Forward trajectories starting at 0000 UTC 12 May 10
GDAS Meteorological Data
Source at 36.05 N 140.13 E
Meters AGL
10878
6666
10000
8000
6000
4000
05/13 05/14 05/15 05/16 05/17 05/18 05/19 05/20 05/21

WRF_OUT

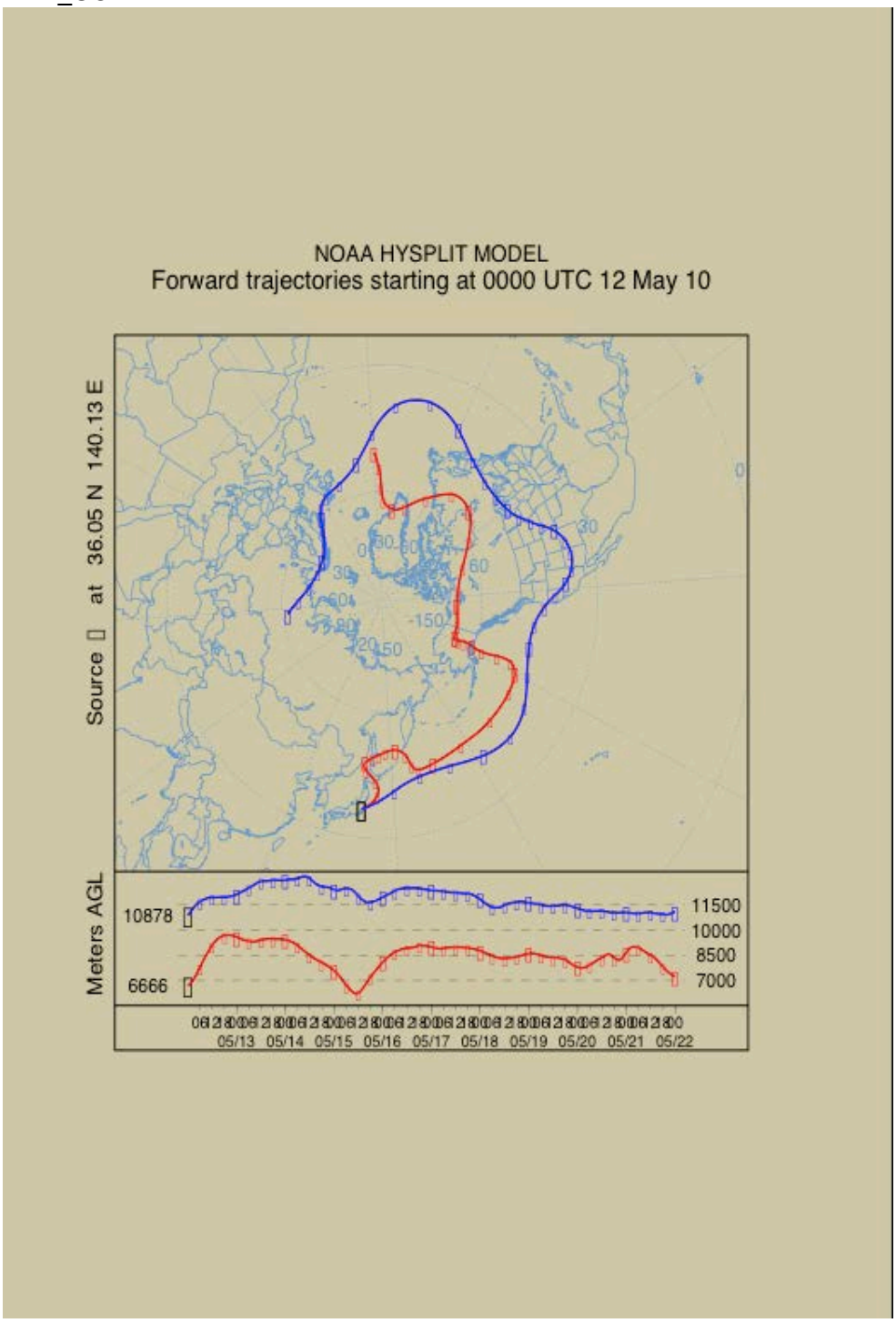
NOAA HYSPLIT MODEL
Forward trajectories starting at 0000 UTC 12 May 10
Source at 36.05 N 140.13 E
Meters AGL
10878
6666
11500
10000
8500
7000
05/13 05/14 05/15 05/16 05/17 05/18 05/19 05/20 05/21 05/22

WRF_OUT (RED TRAJECTORY)

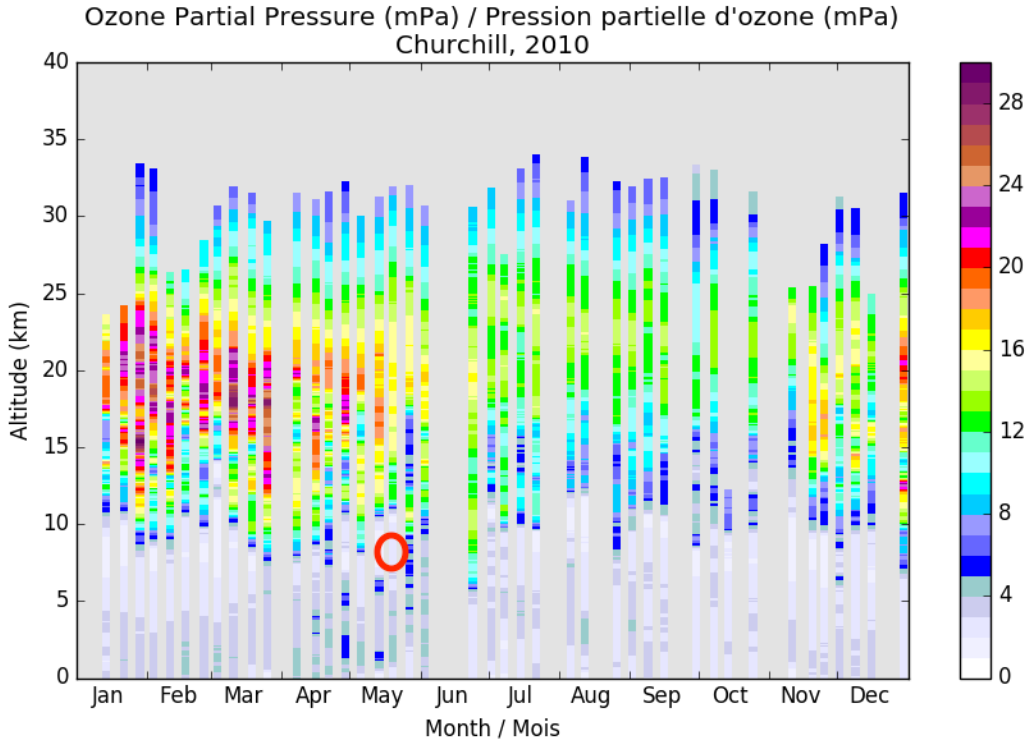

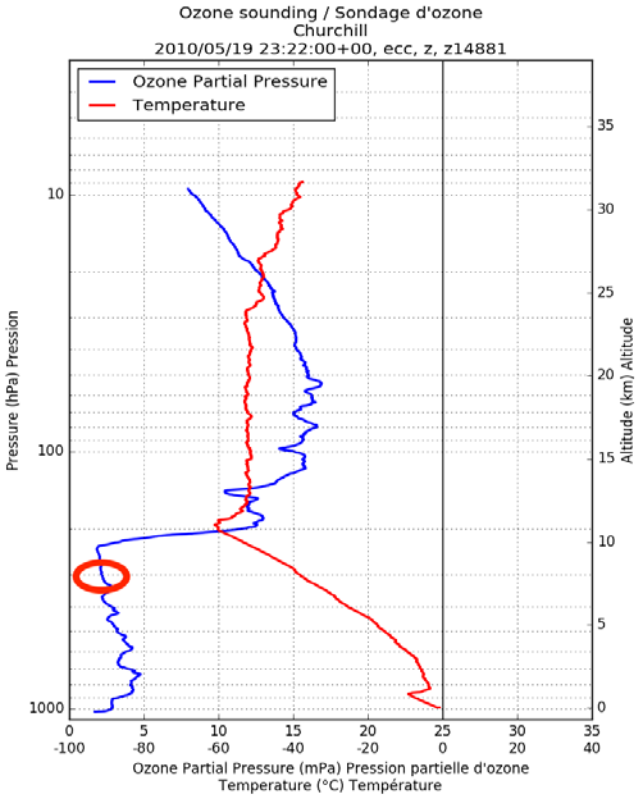

GDAS AND WRF_OUT (BLUE TRAJECTORIES)

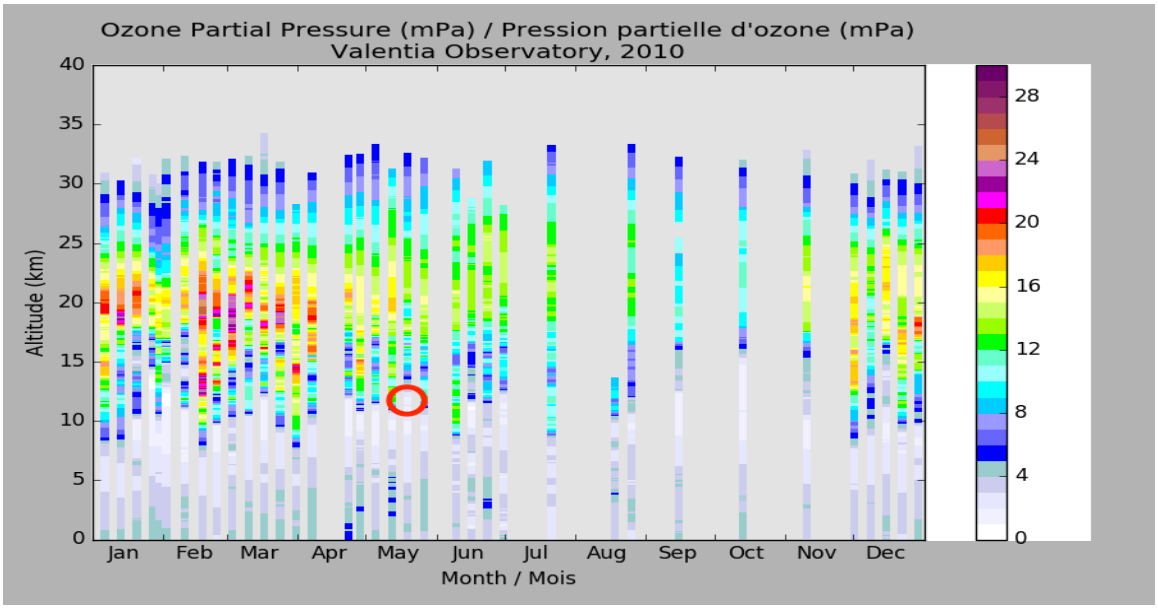
Ozone Partial Pressure (mPa) / Pression partielle d'ozone (mPa)
Valentia Observatory, 2010
Altitude (km)
Month / Mois
Jan
Feb
Mar
Apr
May
Jun
Jul
Aug
Sep
Oct
Nov
Dec

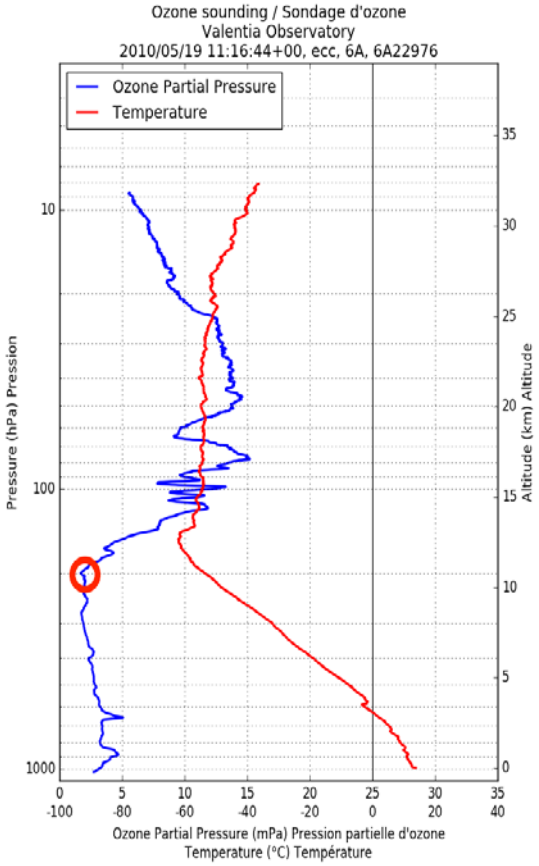
Ozone sounding / Sondage d'ozone
Valentia Observatory
2010/05/19 11:16:44+00, ecc, 6A, 6A22976
Ozone Partial Pressure
Temperature
Pression (hPa) Pression
Altitude (km) Altitude
Ozone Partial Pressure (mPa) Pression partielle d'ozone
Temperature (°C) Température

Trial 3 (4.3)

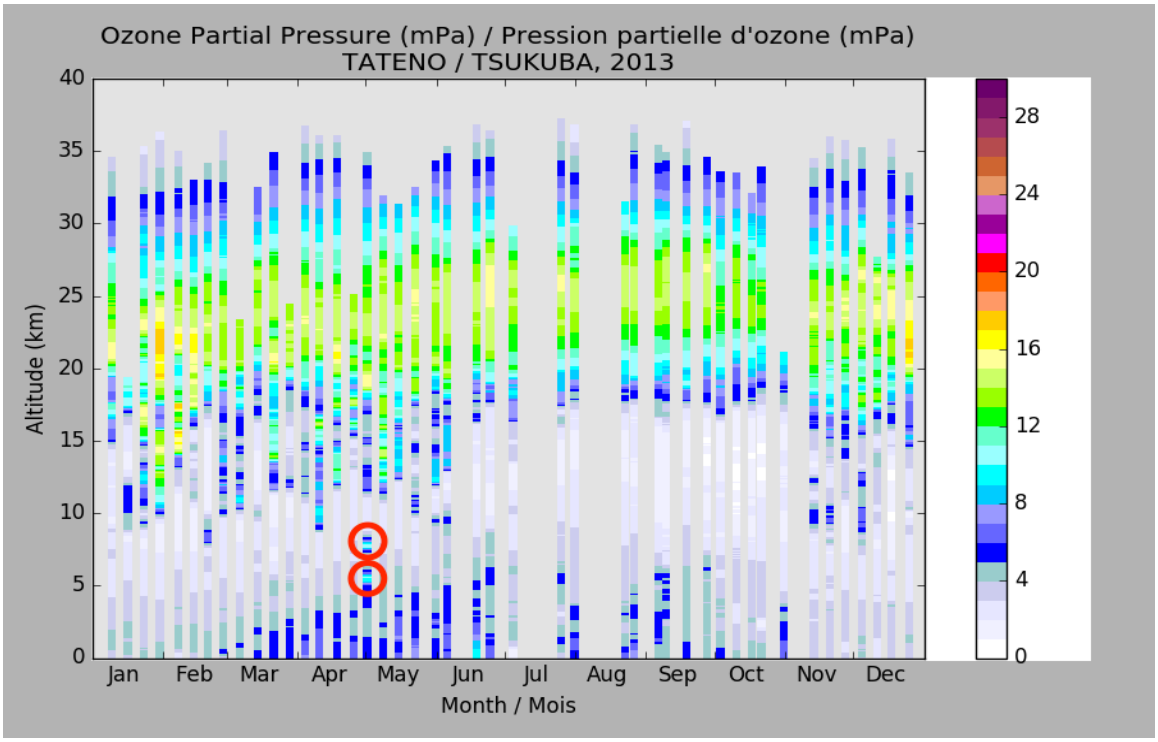
Ozone Partial Pressure (mPa) / Pression partielle d'ozone (mPa)
TATENO / TSUKUBA, 2013
Altitude (km)
0
5
10
15
20
25
30
35
40
Jan
Feb
Mar
Apr
May
Jun
Jul
Aug
Sep
Oct
Nov
Dec
Month / Mois
0
4
8
12
16
20
24
28

GDAS

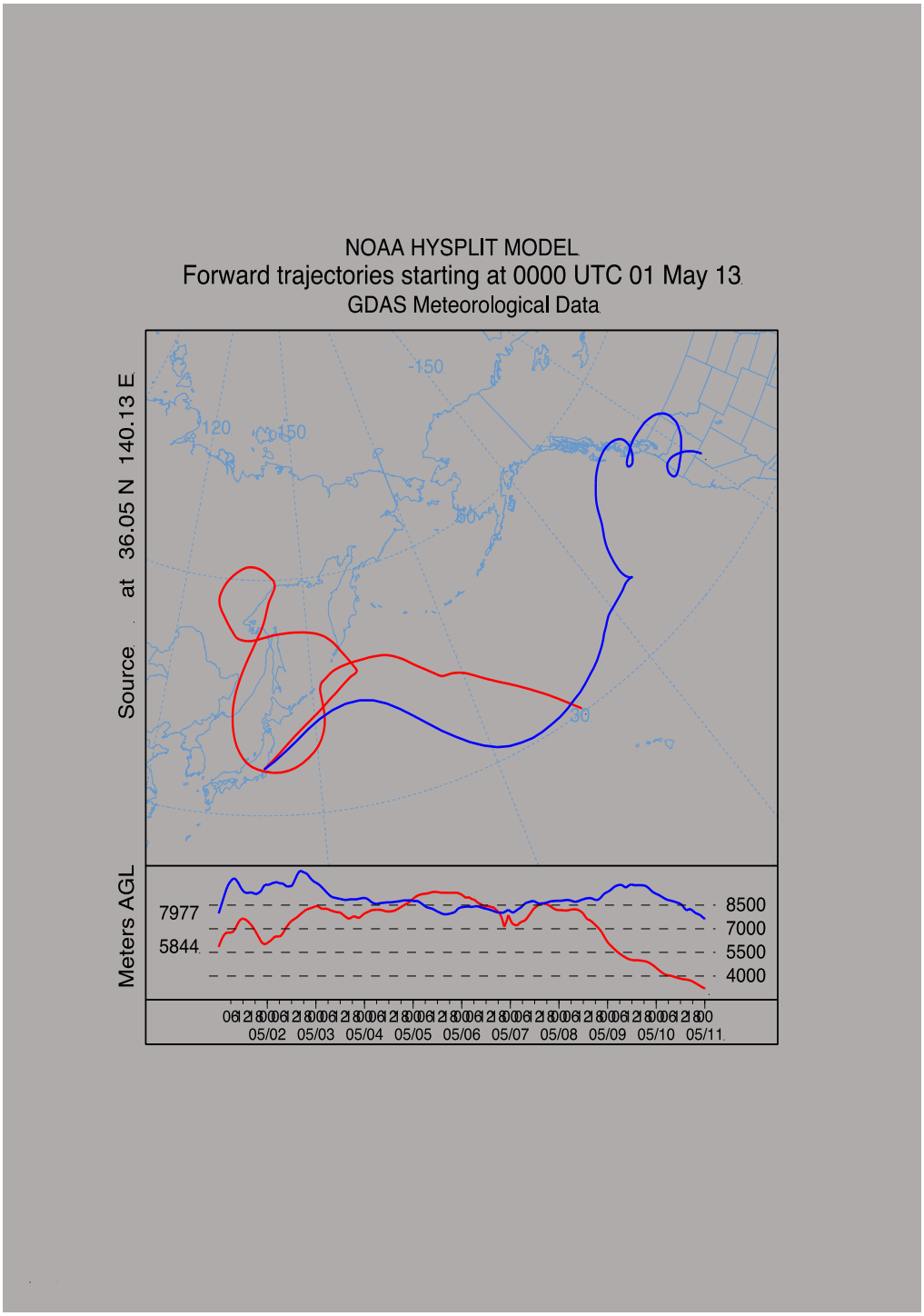
NOAA HYSPLIT MODEL
Forward trajectories starting at 0000 UTC 01 May 13
GDAS Meteorological Data
Source at 36.05 N 140.13 E
-150
120
150
-30
Meters AGL
7977
5844
8500
7000
5500
4000
05/02 05/03 05/04 05/05 05/06 05/07 05/08 05/09 05/10 05/11

WRF_OUT

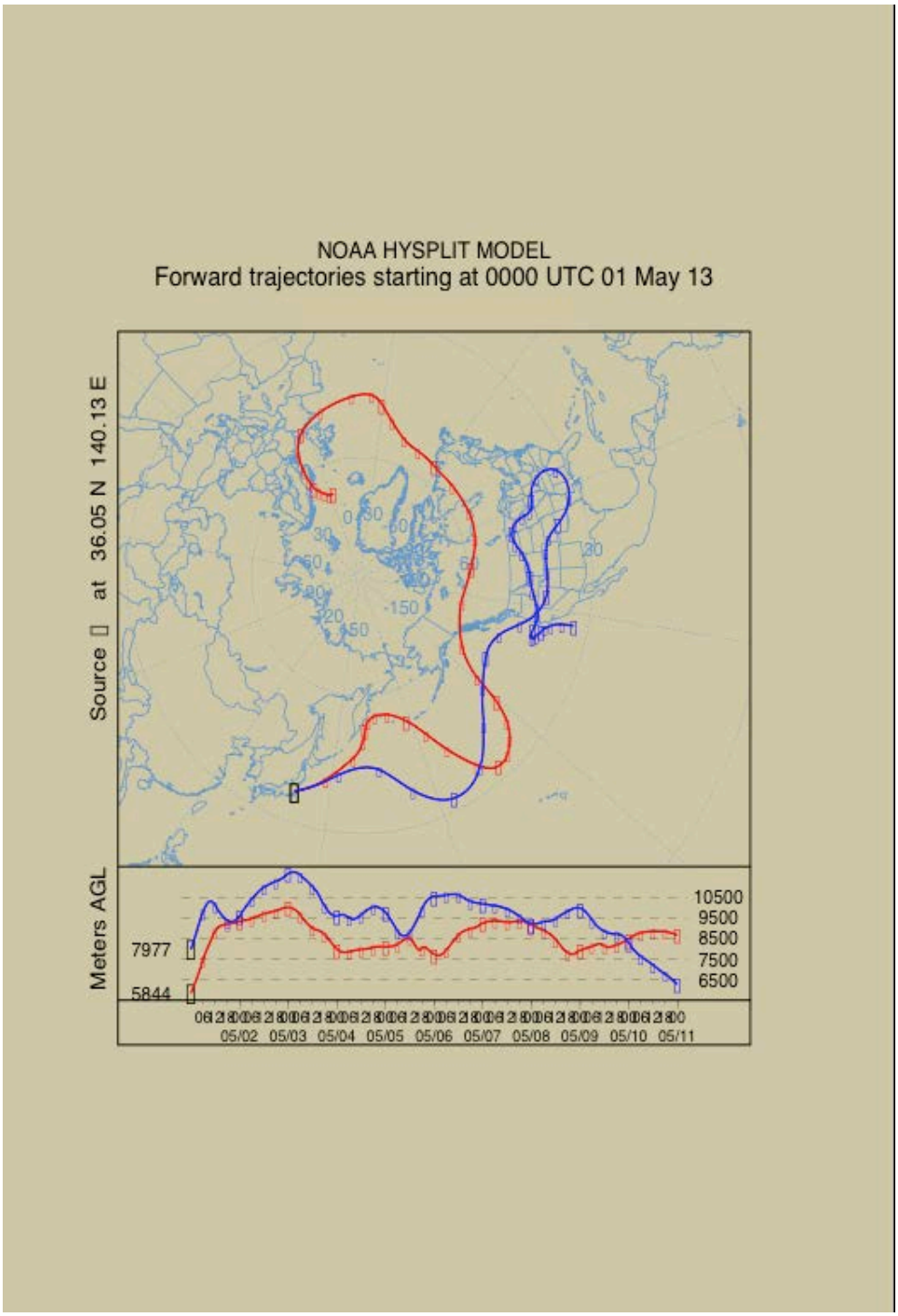

GDAS (BLUE TRAJECTORY)

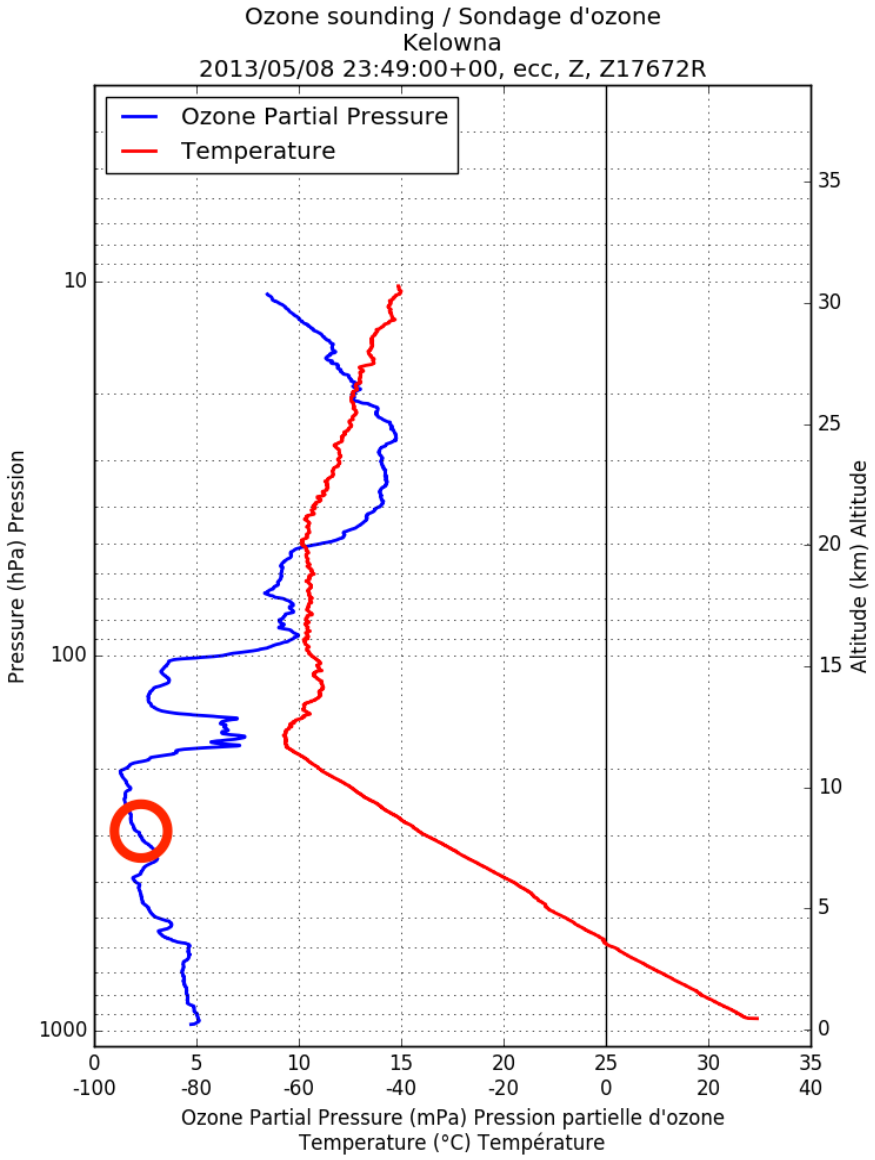

WRF_OUT (RED TRAJECTORY)

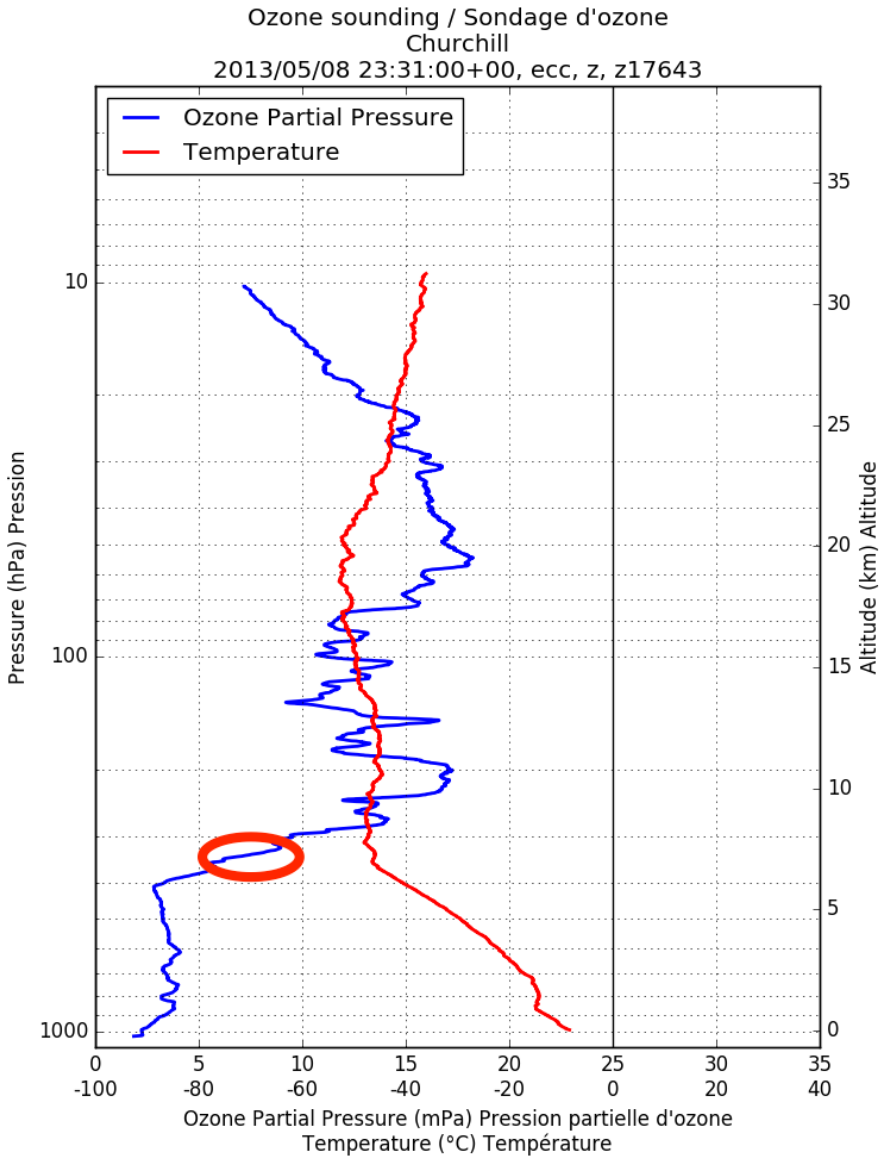

WRF_OUT (RED TRAJECTORY)

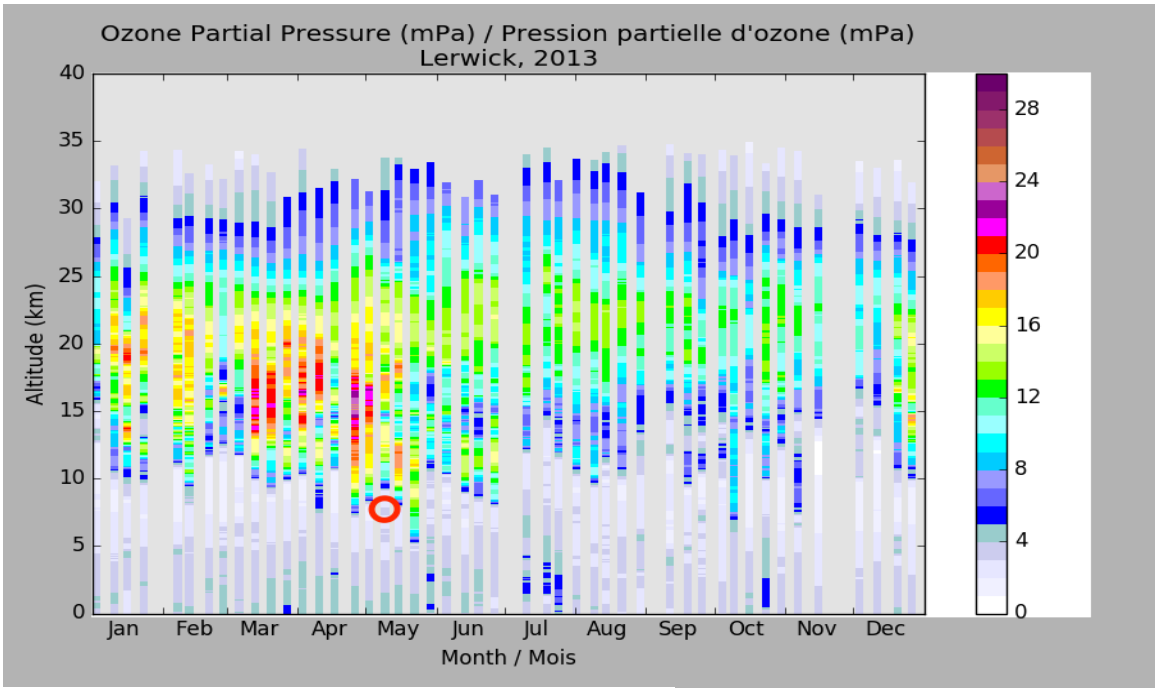

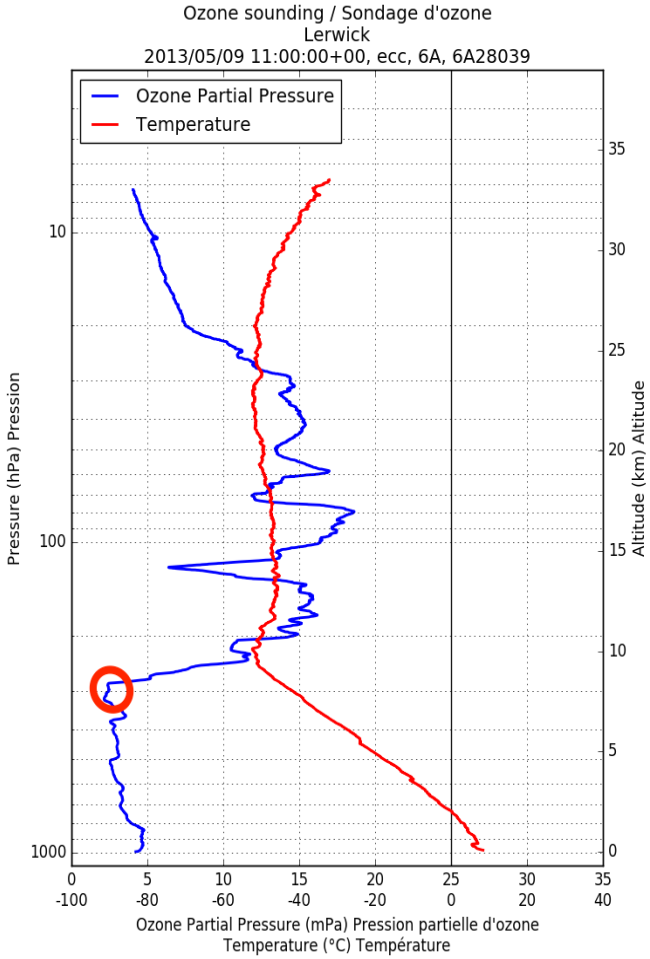

Bodega Bay First Ozone Sounding

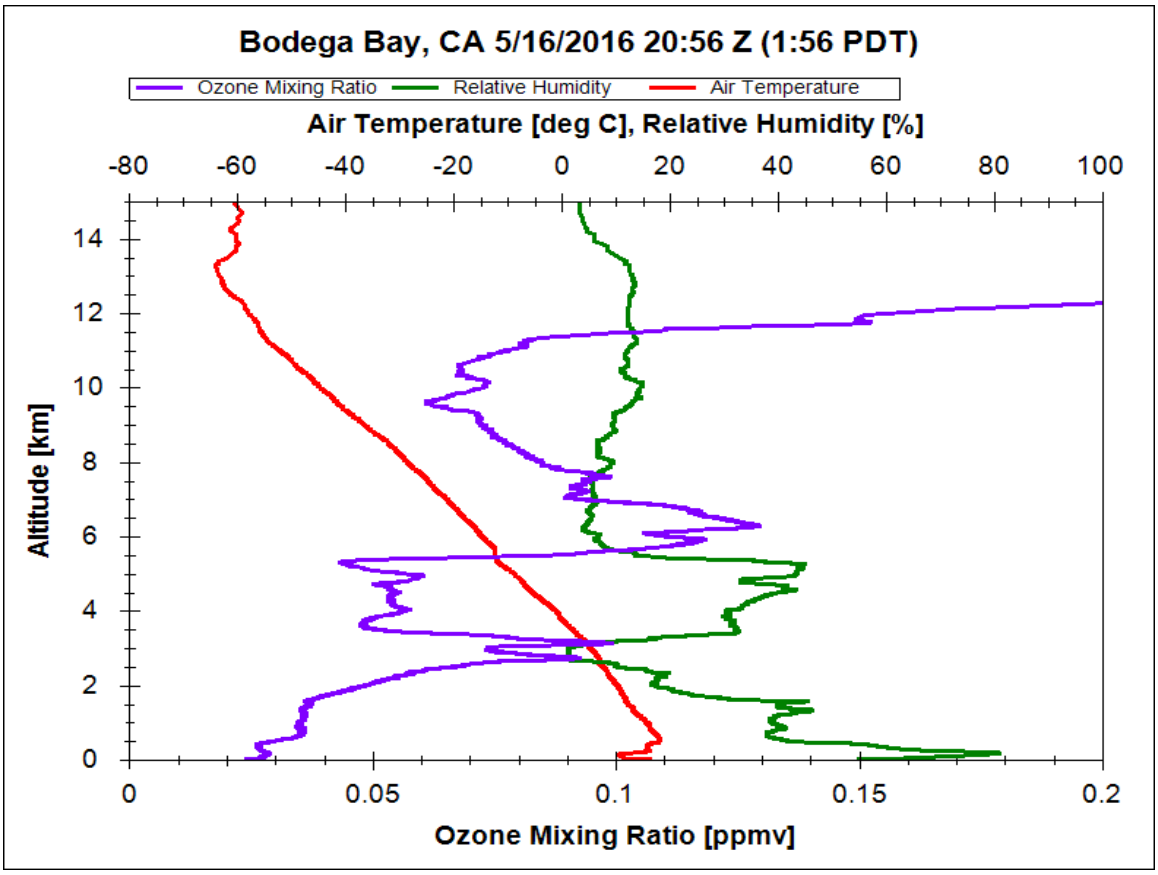
Bodega Bay, CA 5/16/2016 20:56 Z (1:56 PDT)
Ozone Mixing Ratio
Relative Humidity
Air Temperature
Air Temperature [deg C], Relative Humidity [%]
-80
-60
-40
-20
0
20
40
60
80
100
Altitude [km]
14
12
10
8
6
4
2
0
0
0.05
0.1
0.15
0.2
Ozone Mixing Ratio [ppmv]